43384

National Library of Canada / Bibliothèque nationale du Canada

CANADIAN THESES ON MICROFICHE / THÈSES CANADIENNES SUR MICROFICHE

NAME OF AUTHOR/*NOM DE L'AUTEUR* BRUNO QUENTIN DE LORENZIS

TITLE OF THESIS/*TITRE DE LA THÈSE* TIME-DEPENDENT BEHAVIOUR OF ICE-ACCRETION ON A NON-ROTATING CYLINDER

UNIVERSITY/*UNIVERSITÉ* UNIVERSITY OF ALBERTA

DEGREE FOR WHICH THESIS WAS PRESENTED/ *GRADE POUR LEQUEL CETTE THÈSE FUT PRÉSENTÉE* MASTER OF SCIENCE IN METEOROLOGY

YEAR THIS DEGREE CONFERRED/*ANNÉE D'OBTENTION DE CE GRADE* 1979

NAME OF SUPERVISOR/*NOM DU DIRECTEUR DE THÈSE* DR. E. P. LOZOWSKI

Permission is hereby granted to the NATIONAL LIBRARY OF CANADA to microfilm this thesis and to lend or sell copies of the film.

The author reserves other publication rights, and neither the thesis nor extensive extracts from it may be printed or otherwise reproduced without the author's written permission.

L'autorisation est, par la présente, accordée à la BIBLIOTHÈQUE NATIONALE DU CANADA de microfilmer cette thèse et de prêter ou de vendre des exemplaires du film.

L'auteur se réserve les autres droits de publication; ni la thèse ni de longs extraits de celle-ci ne doivent être imprimés ou autrement reproduits sans l'autorisation écrite de l'auteur.

DATED/*DATÉ* May 29 SIGNED/*SIGNÉ* B. de Lorenzis

PERMANENT ADDRESS/*RÉSIDENCE FIXE* 46 Hill Drive
Aurora, Ontario

NL-91 (3-74)

National Library of Canada

Cataloguing Branch
Canadian Theses Division

Ottawa, Canada
K1A 0N4

Bibliothèque nationale du Canada

Direction du catalogage
Division des thèses canadiennes

NOTICE

The quality of this microfiche is heavily dependent upon the quality of the original thesis submitted for microfilming. Every effort has been made to ensure the highest quality of reproduction possible.

If pages are missing, contact the university which granted the degree.

Some pages may have indistinct print especially if the original pages were typed with a poor typewriter ribbon or if the university sent us a poor photocopy.

Previously copyrighted materials (journal articles, published tests, etc.) are not filmed.

Reproduction in full or in part of this film is governed by the Canadian Copyright Act, R.S.C. 1970, c. C-30. Please read the authorization forms which accompany this thesis.

THIS DISSERTATION
HAS BEEN MICROFILMED
EXACTLY AS RECEIVED

AVIS

La qualité de cette microfiche dépend grandement de la qualité de la thèse soumise au microfilmage. Nous avons tout fait pour assurer une qualité supérieure de reproduction.

S'il manque des pages, veuillez communiquer avec l'université qui a conféré le grade.

La qualité d'impression de certaines pages peut laisser à désirer, surtout si les pages originales ont été dactylographiées à l'aide d'un ruban usé ou si l'université nous a fait parvenir une photocopie de mauvaise qualité.

Les documents qui font déjà l'objet d'un droit d'auteur (articles de revue, examens publiés, etc.) ne sont pas microfilmés.

La reproduction, même partielle, de ce microfilm est soumise à la Loi canadienne sur le droit d'auteur, SRC 1970, c. C-30. Veuillez prendre connaissance des formules d'autorisation qui accompagnent cette thèse.

LA THÈSE A ÉTÉ
MICROFILMÉE TELLE QUE
NOUS L'AVONS REÇUE

NL-339 (3/77)

THE UNIVERSITY OF ALBERTA

TIME-DEPENDANT BEHAVIOUR OF ICE ACCRETION ON A NON-ROTATING CYLINDER

by

© Bruno Q. de Lorenzis

A THESIS

SUBMITTED TO THE FACULTY OF GRADUATE STUDIES AND RESEARCH

IN PARTIAL FULFILMENT OF THE REQUIREMENTS FOR THE DEGREE

OF MASTER OF SCIENCE

IN

METEOROLOGY

DEPARTMENT OF GEOGRAPHY

EDMONTON, ALBERTA
FALL, 1979

THE UNIVERSITY OF ALBERTA

FACULTY OF GRADUATE STUDIES AND RESEARCH

The undersigned certify that they have read, and recommend to the Faculty of Graduate Studies and Research, for acceptance, a thesis entitled Time-dependant Behaviour of Ice Accretion on a Non-rotating Cylinder submitted by Bruno Q. de Lorenzis
in partial fulfilment of the requirements for the degree of Master of Science (Meteorology)

Edward Lozowski
.....
Supervisor

Tony Forest
.....

E. Reinelt
.....

Date..May.25.,..1979....

Dedicated to

Heather and Damian

for their love and understanding

Abstract

A model for ice accretion on a cylinder in a water-droplet cloud has been extended to include time-dependence of the growth of the accretion, through empirical methods. To this end 12 experiments were performed with the following range of atmospheric parameters; temperature from -5 to -10 C, liquid water content from .69 to 2.13 g m and airspeed from 15 to 45 m sec . A "shield" technique was devised to facilitate the analysis of the time-dependent behaviour of the growth. It was found that the model consistently underpredicted the growth rate by a factor of two compared to the observed growth rate at corresponding atmospheric conditions. The prediction of the shape of the accretion was found to be substantially improved when the direction of growth was taken to be that inferred from the "bubble lines" present in the accretion rather than the simpler method of radial growth. Discrepancies in the predicted mass and shape were deemed to be at least partially due to the exclusion of spongy ice from the model.

Acknowledgements

The author wishes to thank Dr. E.P. Lozowski for his invaluable guidance and supervision of this thesis. He is also grateful to the Department of Mechanical Engineering and the Mechanical Engineering shop staff for the use and maintenance of their "FROST" Tunnel which was essential for the completion of the experimental portion of this work. Thanks are also extended to the Cartography and Photograpic services of the Department of Geography for their patience and assistance in the production of this thesis.

Table of Contents

Chapter Page

1. INTRODUCTION.....1
2. MODEL DESCRIPTION.....4
3. APPARATUS.....11
   3.1 TUNNEL.....11
   3.2 SPRAY SYSTEM.....13
   3.3 OILED SLIDE.....15
   3.4 ROTATING CYLINDER.....17
   3.5 WIND SPEED.....18
   3.6 TEMPERATURE.....19
   3.7 SHIELD.....19
4. EXPERIMENT.....22
   4.1 DESIGN.....22
   4.2 EXPERIMENTAL PROCEDURE.....23
      4.2.1 Measurement of LWC.....24
      4.2.2 Spray bars.....26
      4.2.3 Accretion.....26
      4.2.4 Removal.....27
      4.2.5 Droplet spectrum.....28
   4.3 DATA RETRIEVAL.....28
      4.3.1 Data extraction from the oiled slides.....28
      4.3.2 Obtaining Cross-sections.....29
      4.3.3 Data extraction from the cross-sections.....31
5. RESULTS.....34
   5.1 BUBBLE LINES.....34

5.2 MASS.....37

5.3 SHAPE OF THE ACCRETION.....40

6. DISCUSSION.....57

6.1 MASS PREDICTION.....57

6.2 SHAPE PREDICTION.....62

7. CONCLUSION.....66

References.....69

Appendix 1.....72

Appendix 2.....75

Appendix 3.....77

Appendix 4.....81

Appendix 5.....83

Appendix 6.....90

List of Tables

Table		Page
4.1	Atmospheric conditions and duration of run.....	24
4.2	LWC measured for each nozzle and the Ludlam Limit for each run.....	25
4.3	Droplet spectra.....	30
4.4	Mass per cm along the cylinder inferred from planimetering the cross-sections.....	31
5.1	Results of the linear regression of φ_{jt} and α_{jt}	35
6.1	Overall collection efficiencies and growth rates for each run.....	58

List of Figures

Figure		Page
2.1	Runs at -5°C	7
2.2	Runs at -10°C	8
3.1	Plan view of the "Frost" Tunnel	12
3.2	Example of oiled slide microphotograph (run 11)	16
3.3	View of working section with shield and test cylinder in place	20
4.1	Schematic representation of angles deduced from bubble lines and growth lines	33
5.1	Intercept of regression γ_{ot} versus time	36
5.2	Slope of regression $\frac{d\gamma}{dt}$ versus time	36
5.3	Observed mass versus time for runs at -5°C	38
5.4	Observed mass versus time for runs at -10°C	38
5.5	Method of interpolation for directional and radial growth technique	41
5.6	Run 1 plots of growth lines, observed (upper lines) and predicted (lower lines) and the plot of ratio of measured to observed thickness $\frac{r_m}{r_o}$ versus angle around cylinder γ	44
5.7	Run 2, as for figure 5.6	45
5.8	Run 3, as for figure 5.6	46
5.9	Run 4, as for figure 5.6	47
5.10	Run 5, as for figure 5.6	48
5.11	Run 6, as for figure 5.6	49

5.12 Run 7, as for figure 5.6..... 50

5.13 Run 8, as for figure 5.6..... 51

5.14 Run 9, as for figure 5.6..... 52

5.15 Run 10, as for figure 5.6..... 53

5.16 Run 11, as for figure 5.6..... 54

5.17 Run 12, as for figure 5.6..... 55

5.18 Run 12, as for figure 5.6..... 56

6.1 Observed growth rate versus free stream flux..... 60

6.2 Model predicted growth rate versus free stream flux..... 60

1. INTRODUCTION

The study of the accretion of ice on a cylinder has traditionally been undertaken as a first step towards understanding the physics of the growth of a hailstone. Because of this, many experiments and theories dealing with the accretion of ice on a cylinder (Ashworth and Knight, 1978), have dealt with a rotating cylinder in an attempt to account for the aerodynamic tumbling of a hailstone.

Another practical problem that requires an understanding of the behaviour of ice accretion is aircraft icing. Specifically, helicopter rotors are very susceptible to icing (Lozowski Stallabrass and Hearty,1979), due to the use of helicopters in the lower levels of the atmosphere where the problem of icing is most severe, and because the slow vertical velocities of which helicopters are capable prevents them from travelling through the area of severe icing quickly. Although the overall approximation of a helicopter rotor (airfoil), by a cylinder would be a gross assumption, Stallabrass(1958) has in fact used a cylinder of equivalent radius of curvature to that of the leading edge of an airfoil to calculate the rate of icing at the airfoil stagnation line. The problem of the rotation of the rotor about a vertical axis introduces complications which are best ignored at present in light of the lack of a true understanding of ice accretion in the far simpler

non-rotating frame.

A similar problem and one no less important is the problem of the icing of a cable (Poots and Rodgers,1975) and specifically power lines, which are essentially cylinders if one ignores the irregularities introduced by twining, and the curvature of the cable hanging under gravity. Power lines are also effectively stationary if one ignores aerodynamic motion. For this problem especially then, one should be able to develop a good understanding of the accretion of ice through the examination of the process of ice accretion on a non-rotating cylinder.

The accretion process needs to be considered in light of its effect on the iced object. For the purpose of aircraft icing the prime consideration is the shape of the accretion and its effect on the aerodynamics of flight. On the other hand when considering the effect on power lines or other stationary structures, the main concern is the amount or mass of ice. Ideally, it would be most advantageous to be capable of predicting both the shape and size of the accretion simultaneously; however, it is nevertheless useful to be able to predict either one or the other independently.

The approach to the problem of understanding the behaviour of the accretion of ice on a cylinder taken by Lozowski et al.(1979), was the development of a purely theoretical model and subsequent comparison of the predicted shapes to those of accretions obtained under controlled conditions in an icing tunnel. This comparison showed that

the model behaved very well for dry growth when water drops in the spray freeze almost immediately on impact and therefore remain very close to where they impinge. But it gave generally poor results for wet growth, for which the droplets impinging on a surface take somewhat longer to freeze and consequently are subject to movement along the surface after impingement.

The approach used in this thesis is one which incorporates both theory and experiment in an attempt to examine the time-dependence of the growth of ice on a non-rotating cylinder. A complete description of the theory used in the development of the basic model can be found in Lozowski et al.(1979), and a brief description of the theory and model will be given in Chapter 2. Following this a description of the apparati used in the experiment is given in Chapter 3 and a discussion of the experimental set-up and procedure is provided in Chapter 4 along with the method of data retrieval. Results are found in Chapter 5, while a discussion of the results and the conclusions are included in Chapters 6 and 7 respectively.

2. MODEL DESCRIPTION

The model calculates ice accretion rates as a function of angle around a non-rotating, unheated, circular cylinder in a supercooled water droplet cloud. The model assumes that a steady-state thermodynamic balance exists at each point over the entire front half of the upstream cylinder face with no variation along the longitudinal axis of the cylinder. The sum of the heat source and sink terms in the steady state heat balance equation is assumed to be zero. For the purpose of model calculations the cylinder, between the stagnation line and the top of the cylinder, is divided into "sectors" of a uniform size as described later in this chapter.

The heat balance equation used was that for liquid water accretion with the provision that water not frozen in a particular sector was allowed to flow back into the next downstream sector. This equation, a detailed discussion of which is found in Appendix 3, consists of eight heat flux terms:

$$Q_c + Q_{lv} + Q_i + Q_{li} + Q_a + Q_{ke} + Q_r + Q_{in} = 0 \qquad (2.1)$$

where:

Q_c represents conduction and convection of heat through the boundary layer of the cylinder.

Q_{lv} represents latent heat transfer due to evaporation and sublimation.

Q_i represents warming of the accreted water to the equilibrium surface temperature.

Q_{lfi} represents the latent heat of fusion released by the fraction of impinging water which freezes.

Q_a represents aerodynamic heating due to adiabatic compression of the air and viscous work in the boundary layer.

Q_{ke} represents kinetic energy of the impinging water droplets. All of this energy is assumed to be converted to heat.

Q_r represents cooling of the runback water to the temperature of the sector into which it flows.

Q_{lfr} represents the latent heat of fusion released by the fraction of runback water which freezes. Since the freezing fraction is calculated with respect to the total water available in a sector it will be the same for both the impinging and runback fluxes.

This equation is solved numerically for the equilibrium surface temperature (T_s) or for the freezing fraction (M) by Newton's method. The solution must fall into one of three thermodynamic zones.

ZONE 1 Dry growth T_s <0 C m =1

All impinging water droplets freeze on contact and remain in the sector into which they impinged. Splashing and spreading of the droplets are ignored.

ZONE 2 Wet growth T_s =0 C m <1

A fraction (m) of the total water available in a particular sector freezes. The remaining liquid water is allowed to run back into the next downstream sector.

ZONE 3 No growth T_s >0 C m =0

No accretion occurs in the sector and all the water is allowed to run back into the next downstream sector. If the sector in question is the sector at the top of the cylinder, the excess water is simply shed into the stream.

Calculations are actually performed for only a quarter of the cylinder because symmetry is assumed about the stagnation line. Gravity effects are ignored as well as any accretion on or runback to the rear half of the cylinder. This appears to be reasonable from observations during the experiment which showed that any accumulation of ice on the rear of the cylinder was insignifigant compared to that on the front half of the cylinder. It is assumed that any liquid water present in the sector at the top of the cylinder is shed into the airstream. This was also borne out for the most part by observation during the experiment. As

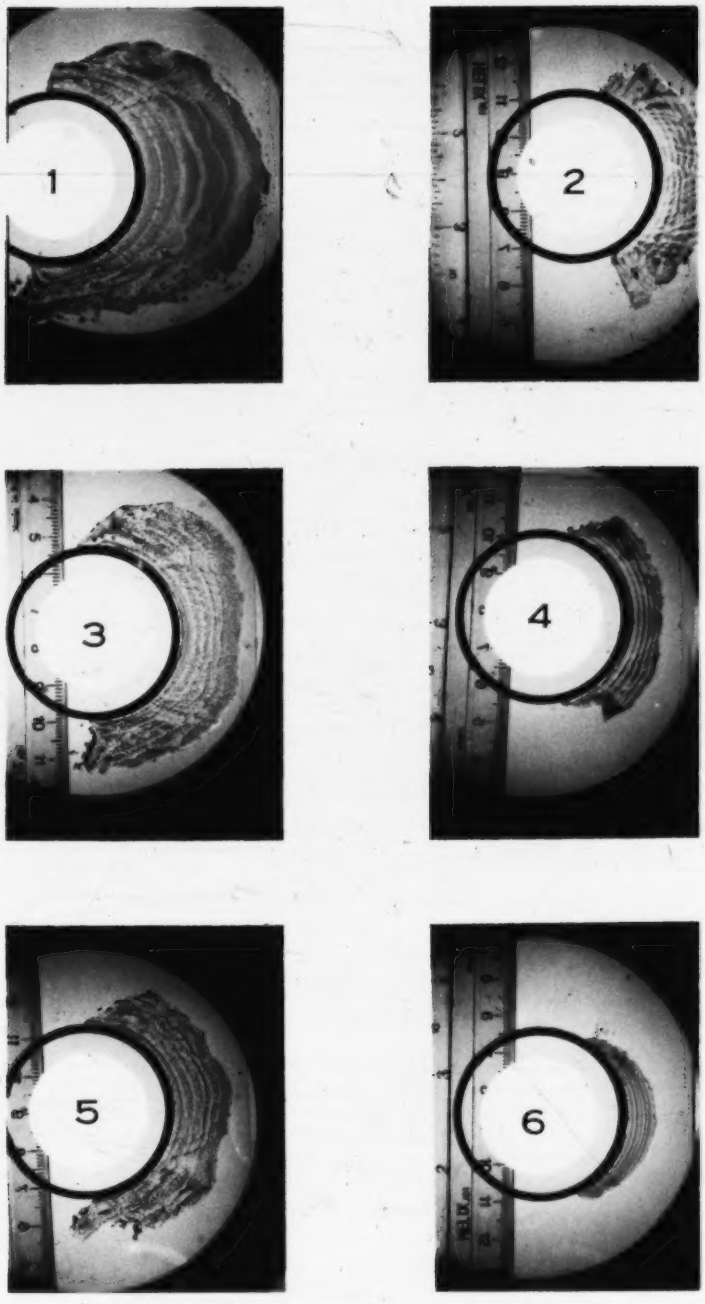

Figure 2.1 Runs at -5°C. Atmospheric parameters for runs are found in Table 4.1

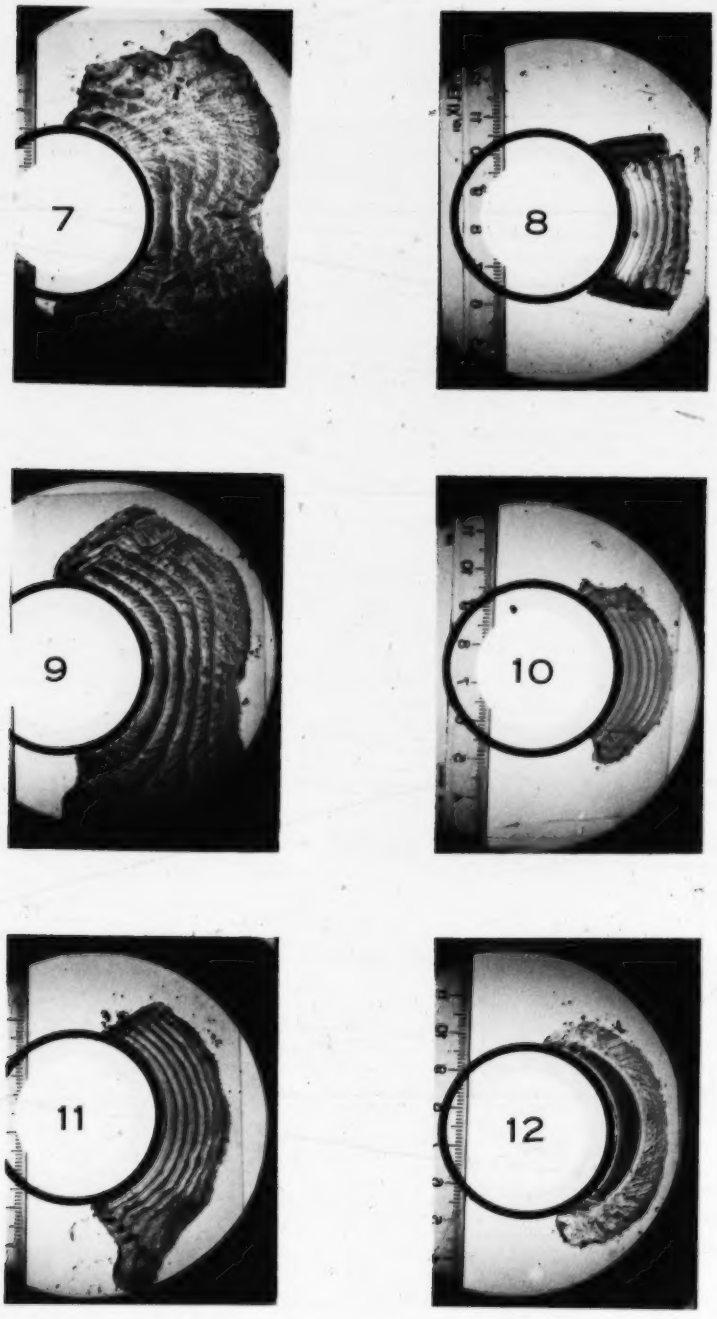

Figure 2.2 Runs at -10°C. Atmospheric parameters for runs are found in Table 4.1

is apparent from Figures 2.1 and 2.2, symmetry about the stagnation line is not always a good assumption. It is felt however that the inclusion of gravity effects would introduce complications at this stage which are unwarranted when considering other assumptions in this thesis. The model has no provision for the consideration of spongy ice, which consists of liquid water in a lattice of ice, although this effect is examined in Chapter 6. A detailed description of the model is found in Appendix 3, and a complete listing of the program in Appendix 5. The definitions of all symbols used in the model are found in Appendix 1.

The input parameters to the program are:

Air temperature (T_a), liquid water content (LWC), cylinder diameter (D_o), and free stream velocity (V).

A choice of rough or smooth heat transfer characteristics is possible, although only the rough characteristic needs to be considered for the experiments performed here (Zukauskas,1972).

Droplet size distribution, expressed as a percent of the total volume in each size category (k). The droplet size distribution was divided into twenty categories at 10μm intervals, centered on 10,20,30...200μm. All the droplets in a category are assumed to have the mean diameter.

Sector size ($\Delta\varphi$). The surface of the cylinder is divided into sectors with arc length ($\frac{D_o \Delta\varphi}{2}$), with the first sector centered on the stagnation line of the cylinder, in order to avoid extrapolation to the stagnation line.

The output of the model which is used to drive the growth subroutine described in Chapter 5, includes the following parameters for each sector:

a. The collection efficiency (β_j).

b. The water flux (F_w (kg $m^{-2} sec^{-1}$)) incident directly from the air stream.

c. The flux of water which has run back from the upstream sector (F_R (kg $m^{-2} sec^{-1}$))

d. The fraction of the total water flux into the sector which is frozen (n).

e. The surface temperature (T_s) of the accretion.

f. The accretion rate (R_i (mm sec^{-1})), assuming the density of ice to be .89 g cm^{-3}.

g. Values for the terms in the heat transfer equation (Equation 2.1).

3. APPARATUS

The experiments consisted of growing ice accretions on an aluminum cylinder of diameter 4.67 cm, in an atmospheric icing wind tunnel. A description of the capabilities and limitations of the tunnel and associated apparatus are presented in this chapter.

3.1 TUNNEL

The icing tunnel was the "FROST" tunnel, which is situated in the Department of Mechanical Engineering, at the University of Alberta. The tunnel was designed by M. Sroka(1972) and Prof. G. Lock. For the purpose of this thesis, only a few salient features will be described.

A plan view of the tunnel is shown in Figure 3.1. The settling chamber of the tunnel, "A", contains eight screens which serve the purpose of creating a uniform wind field across the tunnel and of reducing turbulence. With the sprayers turned off the designer found the turbulence intensity in the working section, "B", to be a maximum of 0.08% at the tunnel's maximum speed of 60 m sec^{-1}. The tunnel has an octagonal cross-sectional shape with a maximum diameter of 1.83 m between opposite surfaces in the settling chamber and a minimum diameter of 0.46 m in the working section, giving the tunnel a contraction ratio of 16.

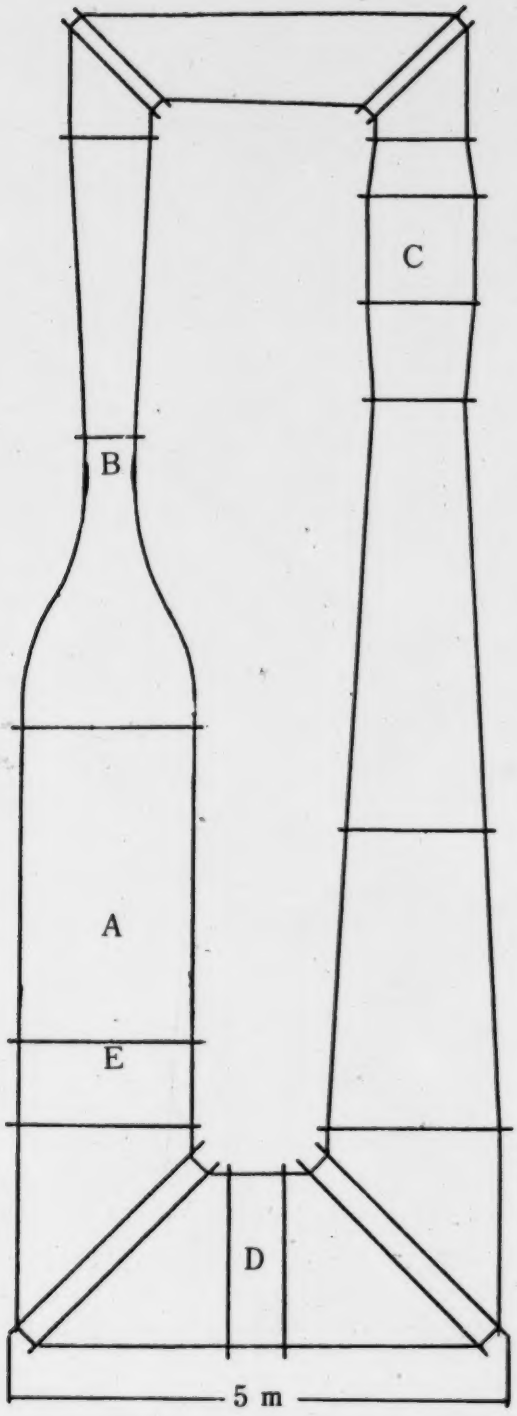

Figure 3.1 Plan view of the "FROST" tunnel (Sroka,1972).

The air is impelled through the tunnel by a 22.4 kW constant speed fan, "C". The speed of the air is controlled by the opening and closing of vanes just upstream of the fan, which restrict the airflow. The air is cooled by a 14.8 kW compressor attached to the cooling coils, "D", upstream of the settling chamber. The tunnel should theoretically be capable of attaining temperatures as low as -20°C (Sroka,1972); however at present about -12°C was found to be the lowest attainable temperature.

3.2 SPRAY SYSTEM

The spray system "E" consisted of seven pneumatic atomizing nozzles of which only two were used at any time. The use of two nozzles proved adequate in providing a uniform liquid water content over an area approximately 4 cm in width by 10 cm high in the working section. This was demonstrated by measuring the ice accretion on a test probe consisting of a non-rotating copper tube 5 mm in diameter inserted horizontally and vertically across the working section through the axis. The deposit thickness on the probe did not vary by more than 10% over the aforementioned distances.

The nozzles were of a coaxial design with the water travelling through the central core and the atomizing air travelling through the outer conduit. Since there was no heater available for the air line and because of the problem of freezing of the nozzles, it was decided to bypass the

water cooling system described by Sroka(1972). This meant that the water entered through the tunnel wall at a temperature of about 20°C. Since the nozzles were located near the center of the tunnel, both the air and the water had to travel about 90 cm down their respective conduits before entering the airstream, so that some cooling of the spray water must have taken place. The pressure of the atomizing air was kept at 1.75×10^5 Pa relative to the pressure in the settling chamber and the adiabatic expansion of this air most probably served to cool the droplets still further. Rough estimates of the cooling due to adiabatic expansion suggest that the temperature of the air leaving the nozzles would be between -30°C and -40°C. This led to the problem of nozzle freezing in both the -5°C and -10°C runs, however there was no evidence that the droplets froze.

It would appear reasonable therefore to assume that the spray was in fact near the ambient temperature of the air stream by the time it reached the working section approximately 2.5 m downstream from the nozzles. Ashworth and Knight(1978) for example have shown that droplets of 200μm diameter reached within 3°C of a free stream temperature of -24°C after only 1.2 m of downstream travel with wind speeds similar to those used in this experiment. According to the manufacturer, the nozzles were capable of producing droplets with diameters of 10μm to 200μm, and this was borne out by the oiled slide samples for most of the runs. The very large drops (>200μm) in some samples

(see Figure 3.2), were considered anomalous and were therefore ignored.

3.3 OILED SLIDE

The droplet spectrum was measured for each run using a glass slide coated with a thin layer of "Shell Omala 85" oil. The slide gun used was that described in Sroka(1972) and the sample was taken in the working section 50 cm upstream of the accretion cylinder. The hydraulics of the gun were not functioning so that its operation had to be performed manually. One source of error in the measurement of the diameters of the droplets is the flattening of the drops due to the thickness of the oil on the slide. It was attempted to keep the oil on the slide at a uniform thickness greater than about 200μm in an attempt to minimize this effect. Another possible error arises from the coalescence of droplets on the slide. Fortunately, as is shown in Chapter 4, reasonable uncertainties in the spectrum of the droplets do not seriously affect the predictions of the model.

An example of a microphotograph made using this technique is found in Figure 3.2. This example was obtained by photographing the oiled slide with transmitted light through a 10X magnifying microscope with Kodak Panatomic-X film exposed for 1/15 sec.

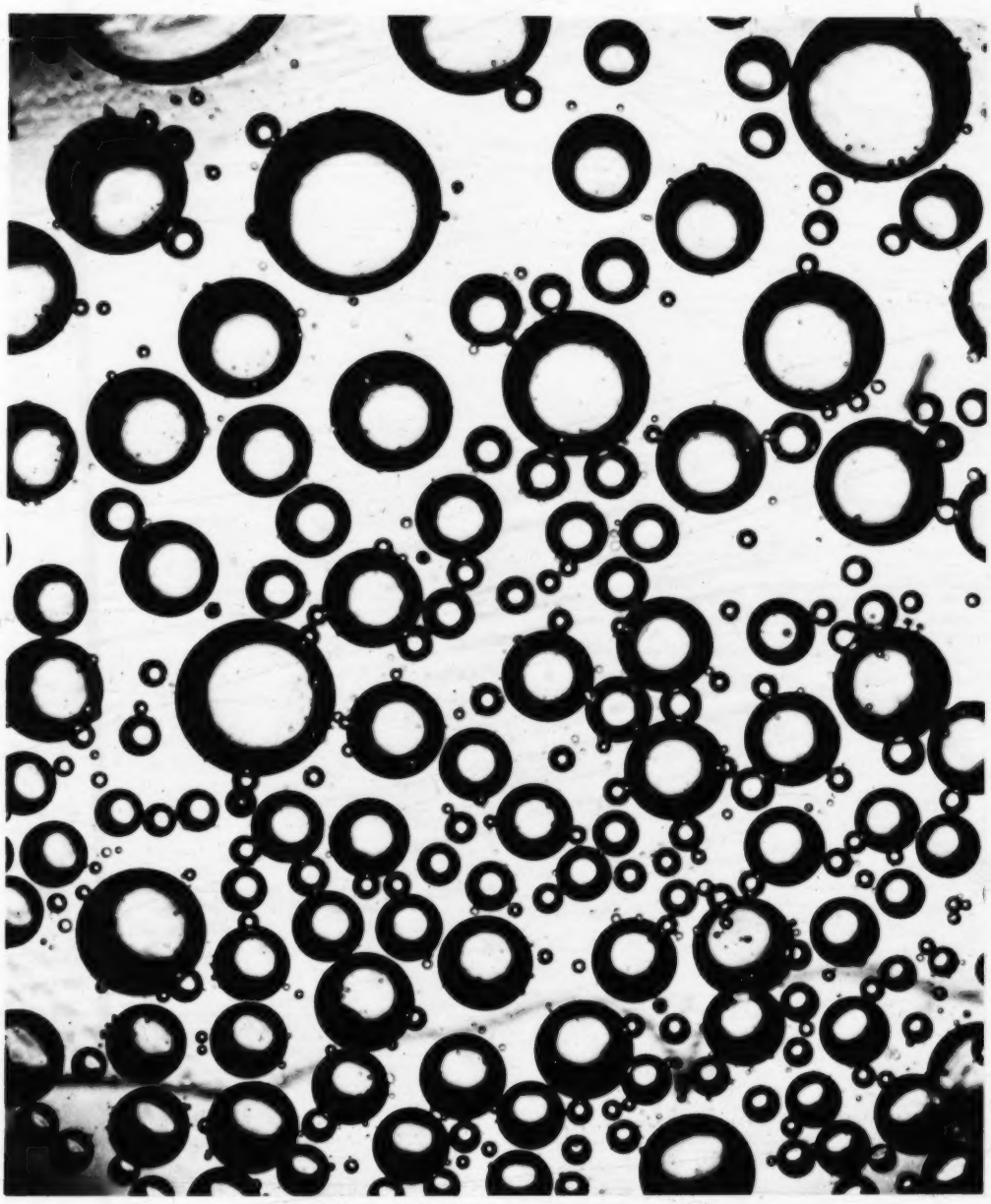

Figure 3.2 Example of oiled slide microphotograph (run 11). Magnification is 100X.

3.4 ROTATING CYLINDER

The LWC was measured using the rotating cylinder method (Stallabrass,1978). A stainless steel cylinder, of 2.79 mm diameter was inserted into the centre of the droplet stream in the working section just ahead of the position of the test cylinder, but without the test cylinder in place. It was rotated at approximately one Hertz for as long as was necessary to achieve a final ice diameter of about 4 mm. The cylinder was then weighed on a balance with a precision of 10^{-6} kg. The development of the formula used to determine the LWC from the mass accreted is found in Appendix 2. This is,

$$LWC = \frac{\pi \rho_i}{2Vt}\left\{\left(\frac{4M}{\pi l \rho_i} + d_o^2\right)^{1/2} - d_o\right\} \qquad (3.1)$$

where the symbols are defined in Appendix 1.

A series of trial runs using the same spray settings were performed to check the temporal stability of the LWC. Measurements were found to be consistent to the nearest 10^{-6} kg for accretions of 10^{-4} kg. The Ludlam limit for the rotating cylinder was calculated using the model. This is the critical LWC which separates the wet and dry growth regimes and above which measurements by the rotating cylinder method become less reliable (Stallabrass,1978). In practice this limit may be exceeded since spongy ice will grow at LWC's slightly higher than this limit. When the temperature at which the Ludlam limit was calculated is exceeded by a degree or two (Stallabrass,1978), splashing

and shedding will occur at a rate sufficient to cause underestimation of the actual LWC.

3.5 WIND SPEED

A Pitot tube was used initially to measure air stream speed. Since this had to be inserted into the stream it was not useful in monitoring the wind speed during a run because of icing. For this reason a Venturi meter was installed between the working section and the settling chamber. The difference in static pressure at the tunnel wall was measured using a water filled manometer and the wind speed was calculated according to the formula:

$$V = \left\{ \frac{597.84\ \Delta p}{\rho_a (1 - \pi_t)^2} \right\}^{1/2} \qquad (3.2)$$

where the symbols are defined in Appendix 1.

This formula assumes that the air is incompressible which may introduce errors that are most likely small since the maximum wind speed was only 45 m sec^{-1}.

Checks were run on the temporal stability of the wind speed. Without icing it was found to vary by less than 1 m sec^{-1} at a speed of 15 m sec^{-1} and by less than 0.25 m sec^{-1} at a speed of 45 m sec^{-1}.

3.6 TEMPERATURE

Temperature was measured by Copper-Constantan thermocouples placed at various points in the tunnel. In order to monitor the airstream temperature continuously, the thermocouple chosen was one immediately upstream from the spray nozzles. This thermocouple was checked against the one in the working section and it was found to give temperatures consistently greater than those in the working section by a value of about .5°C, although this varied somewhat with airspeed. This was assumed to be due to the unbalanced effects of adiabatic expansion in the working section and differences in aerodynamic heating between the sections. The free-stream temperature was initially set using the thermocouple in the working section before the sprayers were turned on. Temporal changes in temperature were held down to 0.5°C by the automatic thermostatic control on the compressor. It was assumed that this was also capable of compensating for the addition of latent heat while the accretion took place.

3.7 SHIELD

In order to study the time variation of the ice accretion it was necessary to devise a method of delineating the growth shape at specified times in a way which would have a minimal effect on the overall accretion. The method of lowering the LWC momentarily to allow dry growth, (Carras, Thwaites and Macklin,1977), was discarded due to

Figure 3.3. View of working section with shield and test cylinder in place.

the difficulty of achieving the same LWC having once reduced it. Also, if the spray output was lowered too much, the nozzle would promptly freeze and thwart the completion of the run. Moreover, apart from the technical difficulty, this method does add some ice to the accretion, albeit a small amount, and consequently changes the shape of the accretion. A second approach was to use a shield to block completely the spray flux to the cylinder for a short interval (Figure 3.3). Preliminary trials were made using the shield to find the optimum time to leave it in place in front of the accretion. It was found that inserting the shield quickly and leaving it in place for 30 seconds resulted in a discontinuity in the opacity of the accretion which outlined the accretion shape at the time of insertion. The physical interpretation of why these lines occur is uncertain, but

Ashworth and Knight,(1978a) suggest that ice will grow opaque at deposit temperatures below -3°C and clear at higher temperatures. It was believed that the insertion of the shield and the cutting off of the water flux and aerodynamic heating due to stream flow caused the ice surface during wet growth to cool to some temperature close to the air temperature. This effect caused the surface of the accretion to change from a clear growth regime (T_s =0°C),to an opaque growth regime (T_s <-3°C), thereby delineating the shape of the accretion at the time of insertion of the shield.

4. EXPERIMENT

4.1 DESIGN

Since the original model (Lozowski et al.,1979), was found to work well for cases where dry growth occurred, it was decided to concentrate on cases that grew wet for at least some portion of the accretion near the stagnation line of the cylinder if not over the entire cylinder. The limitations of the tunnel dictated that only wind speeds of 45 m sec^{-1} or lower could be used, even though the maximum attainable speed without icing was 60 m sec^{-1}. This limit was imposed by the blocking offered by the cylinder itself, by the accretion and by a screen downstream from the working section, used to protect the vanes and impeller from damage due to objects which may become dislodged in the working section. The cooling system was capable of attaining temperatures of -15°C without the sprayers on. With the sprayers on, however, the limit was -12°C, which required approximately two hours to achieve from room temperature.

The most critical tunnel limitation was the rather coarse adjustment mechanisms for the spray bars. Once the flow of water was set it appeared to maintain a constant LWC, but it was virtually impossible to duplicate a LWC value from one run to the next. However, with the presence

of two valves in the water line, it was possible to set the flow with the continuously adjustable downstream valve and then turn the flow off and on with the two-position upstream valve. This made it possible to return to the same LWC during a particular run, which was necessary as is explained later for some rotating cylinder measurements.

Because of the tunnel design limitations and the limitation of time it was decided to perform only twelve runs using three wind speeds, two temperatures and two LWC's. Since the LWC could not be set exactly in advance a relatively high and a relatively low setting were used and the precise values were then measured with the rotating cylinder a priori for each run. Table 4.1 contains the parameters for each of the twelve runs.

The LWC's were set to values considered reasonable for large cumulus and cumulonimbus clouds (Rogers,1976). Values for stratiform clouds are generally much lower.

4.2 EXPERIMENTAL PROCEDURE

The experimental procedure was identical for all runs except number 12 and for some LWC measurements. These differences will be discussed in the appropriate sections.

The general procedure was:

1) Adjustment of the spray bars to give an even spatial distribution of the LWC.
2) Measurement of the LWC, using the rotating cylinder.

Run #	Temp(^{o}C)	V (m sec^{-1})	LWC (g m^{-3})	Duration (min.)
1	-5	45	1.79	12
2	-5	45	0.80	12
3	-5	30	1.54	12
4	-5	30	0.81	12
5	-5	15	2.04	12
6	-5	15	0.75	12
7	-10	45	2.09	12
8	-10	45	0.69	12
9	-10	30	2.13	12
10	-10	30	0.69	12
11	-10	15	1.51	12
12	-10	15	0.73	15

Table 4.1. Atmospheric conditions and duration of run.

3) Alternate insertion of the shield and growth of the accretion.

4) Measurement of the droplet size distribution with an oiled slide sample taken during the accretion.

5) Removal of the accretion for later analysis.

4.2.1 Measurement of LWC

The rotating cylinder method (Stallabrass,1978) was used for finding the LWC of each run. Because of the limitation imposed by the Ludlam limit, which is given for each run in Table 4.2, it was necessary to modify the procedure for runs 1,3,5 and 7. Instead of taking the measurement with both spray bars running, it was necessary

Run #	1	2	3	4	5	6
LWC 1	1.17		0.71		1.06	
LWC 2	0.62	0.80	0.83	0.81	0.97	0.75
Total	1.79	0.80	1.54	0.81	2.04	0.97
Critical LWC	0.85	0.80	1.03	1.04	1.38	1.39

Run #	7	8	9	10	11	12
LWC 1	1.15					
LWC 2	0.94					
Total	2.09	0.69	2.13	0.69	1.51	0.73
Critical LWC	1.77	1.78	2.12	2.13	2.84	2.84

Table 4.2. LWC (g m^{-3}) measured for each nozzle or both as required, and the Ludlam limit (critical LWC) for the rotating cylinder.

to measure the LWC contributed by each spray bar separately, in order not to exceed the Ludlam limit. The results were then added together to give the total LWC for these runs. The spray bars were turned off one at a time using the upstream valve so that the measurement of the LWC from the other could be taken. As can be seen in Table 4.2, the Ludlam limit was exceeded by one of the spray bars in Run 1. This suggests that the estimated LWC for that run is most likely too low. Since there is no way of objectively adjusting the LWC to compensate for this effect it was decided to present this case as it stands, bearing in mind that the measured LWC is low. All other measurements were within the Ludlam limit.

4.2.2 Spray bars

The angle of injection of the droplets from the spray bars was adjusted for every run to give an even distribution of LWC in the center of the working section as described in Chapter 3. This was necessary due to the change in range and trajectory of the droplets with size and with wind speed. The nozzles would get plugged with debris from time to time and had to be replaced. This further complicated matters since the droplet size spectrum was not constant from one nozzle to the next, although as shown in Section 4.3 this did not seriously affect the output of the model.

4.2.3 Accretion

The insertion of the accretion cylinder was performed with the sprayers on, the fan off and the shield in the tunnel. The fan was then turned on and the system allowed to run for one minute before the shield was removed. This was longer than appeared necessary for an steady state to be reached with respect to wind speed, temperature and LWC. The shield was then withdrawn and the accretion allowed to grow for 2 minutes. The shield was then inserted for 30 seconds, and withdrawn. This procedure was repeated every 2 minutes until the accretion had grown for a total of 10 minutes on the cylinder excluding the time the shield was in place. A final 2 minutes of growth was allowed at the end to protect

the 10-minute surface during handling of the accretion. For Run 12, the output from the spray bars was increased substantially after the 10-minute mark and the accretion was allowed to grow for an extended period of time in order to protect the small and apparently fragile accretion of this near dry-growth case.

Throughout each run a constant check was kept on the wind speed via the Venturi meter and on the temperature via the thermocouple. The wind speed control vanes were adjusted as necessary in order to maintain a constant airspeed. It was possible to keep the maximum variation in airspeed down to about 3 m sec^{-1}.

4.2.4 Removal

Upon removal from the tunnel, the cylinder with the accretion still attached was rushed to a cold room kept at -20°C. Cold tap water was poured through the hollow cylinder thereby thawing a thin layer of the accretion next to the cylinder. This allowed the accretion to be pulled away from the cylinder with no damage. In no case did this melting affect the 2-minute or subsequent growth lines, although it most certainly resulted in a change of the inner surface of the accretion, estimated to be of the order of 1 mm or less.

4.2.5 Droplet spectrum

The collection of droplets on the oiled slide was performed during one of the 2 minute accretion intervals. The procedure used is described in Chapter 3. The whole procedure including the photography took about 30 seconds per sample and therefore did not interfere with the monitoring of the tunnel and shield.

4.3 DATA RETRIEVAL

4.3.1 Data extraction from the oiled slides

The photographs of the oiled slides were made into 8X10 prints. The drops were counted and placed into 20 categories 10μm wide centered on 10,20,30...200μm, as required for the program. The 10 m category also contained all drops <5μm in diameter although these were few in number. In some of the samples taken (runs 7, 9 and 11) there were very large drops present. These samples were discarded and the distribution used for runs 7,9 and 11 is the average of all the other runs. The model was used to check the sensitivity of the icing to variations in the droplet size distribution. The extreme case of all drops in the 200μm category gave ice accretion rates that differed by 2.5% at most from those calculated using the average spectrum. It is therefore safe to conclude that substituting an average distribution for

the true distribution in runs 7,9 and 11 probably does not cause serious errors.

The droplet size distributions are given in Table 4.3, and a microphotograph of an oiled slide sample is found in Figure 3.2.

4.3.2 Obtaining Cross-sections

Cross-sections of the accretions were obtained by a procedure described by Ashworth and Knight (1978). This consisted of slicing the accretion with a bandsaw in the center of the section where approximate uniform longitudinal growth occurred. The newly exposed surface was filed smooth and pressed onto a glass slide which had been heated to just above the freezing point. Pressure was maintained for a few seconds to ensure that excess melt-water was ejected from between the slide and the accretion. The accretion attached to the slide was then cut again on the bandsaw so that a thickness of about 3 mm remained on the slide. This section was filed smooth until the growth lines were clearly visible,(usually about 2 mm thick). A ring having the same diameter as the accretion cylinder was placed against the concave part of the section along with a ruler for use later when scaling the section. This was then photographed with transmitted light using a 125 mm Macro lens on Panatomic-X film at f 2.4 and a shutter speed of 1/15 second. In addition, for each sample a cross-section of the accretion 6 mm thick was obtained and weighed on a chemical balance. It

Run # Diam.	1	2	3	4	5	6	8	10	12	7,9,11
10	0.1	0.1	0.1	0.1	0.1	0.1	0.1	0.1	0.1	0.1
20	0.3	0.6	0.1	0.9	0.1	0.1	0.2	0.5	0.2	0.3
30	1.0	2.0	0.5	3.2	0.5	0.5	0.8	1.7	0.8	1.2
40	2.5	4.6	1.1	5.3	0.9	1.3	3.5	2.9	1.4	2.0
50	5.4	7.7	2.0	8.2	1.7	2.4	5.6	5.0	7.5	3.4
60	8.7	11.1	3.0	10.3	2.5	3.6	7.3	6.8	3.8	4.9
70	12.0	13.4	4.3	11.6	3.6	5.2	9.0	8.8	5.4	5.8
80	13.6	13.8	5.5	12.2	4.8	6.4	10.0	9.9	6.6	6.9
90	13.1	13.0	6.5	11.3	6.2	7.8	10.8	10.5	8.0	7.8
100	11.9	11.5	7.2	9.3	7.1	8.9	11.5	11.7	9.5	8.7
110	10.0	9.3	7.6	8.0	7.7	9.4	10.8	11.8	10.3	8.6
120	8.8	6.2	7.9	6.6	7.9	9.7	10.5	11.4	10.1	8.6
130	7.2	4.0	7.8	5.4	8.0	9.8	10.0	10.0	9.3	7.9
140	5.4	2.7	7.5	4.3	7.9	9.3	8.7	9.6	8.7	7.0
150			7.2	3.3	7.7	8.5			7.2	6.7
160			7.1		7.6	7.0			6.5	5.8
170			6.9		7.3	5.6			5.5	5.0
180			6.4		6.9	4.4			4.3	4.2
190			6.0		6.4					3.3
200			5.5		5.5					2.4

Table 4.3. Droplet spectra. Percent volume in a 10μm diameter interval centred on the given diameter. The spectrum for runs 7,9 and 11 is the average of the other spectra.

should be pointed out that the weight of these sections included the 10 to 12 minute extra accretion for runs 1 through 11.

Photographs of the cross-sections for each run are found in Figures 2.1 and 2.2, and the weight per cm along the cylinder for half the cross-section are found in Table 4.4.

Elapsed time (min)	2	4	6	8	10	12
Run #						
1	1.53	3.09	5.19	6.48	9.98	11.73
2	0.64	1.14	1.76	2.44	3.21	3.60
3	0.90	2.04	3.14	4.60	6.18	7.70
4	0.27	0.74	1.40	1.82	2.49	2.60
5	0.58	1.32	2.08	2.82	3.59	5.39
6	0.30	0.56	0.84	1.05	1.30	1.24
7	2.59	5.74	8.58	11.80	14.75	18.19
8	0.52	0.96	1.48	1.98	2.67	3.57
9	1.29	5.07	6.39	9.32	11.87	12.13
10	0.32	0.90	1.20	1.88	2.39	2.62
11	0.88	1.53	2.25	2.91	3.67	5.81
12					1.09	----

Table 4.4. Mass (g cm^{-1}) along the cylinder inferred from planimetering the cross-sections. Density is assumed to be .89 g cm^{-3}.

4.3.3 Data extraction from the cross-sections

The developed film negatives of the cross-sections were mounted in metal slides. They were then projected onto a rear-projection screen and the growth lines were traced onto graph paper. The "bubble lines" were also traced for later analysis. These lines which appear approximately as radial lines in Figures 2.1 and 2.2, are thought to arise from the precipitation of air from the water as the latter freezes thereby trapping the bubbles in the ice. These tend to accumulate in lines separating lobes in the accretion due to the flow of water into the hollows between the lobes and have been observed in naturally occurring hailstones as well as in other accretion experiments. The consensus is

(Macklin,1977; Carte,1961), that these bubble lines indicate the direction of growth of the lobes which they separate. This lobe structure was observed in the wet accretions gathered in this experiment and it is present in runs 2 through 11 in varying degrees of clarity.

The traces of the growth lines were then planimetered to find the area at each time step, and thence the mass. The lines used in planimetering are the leading edge of the dark bands in Figures 2.1 and 2.2. The accretion was assumed to have a density of .89 g cm^{-3},Lozowski et al. (1979). Table 4.4 contains the total mass up to each time step inferred from the planimeter measurements, and the total for the section weighed. The differences between the actual mass and the planimeter-derived total mass are attributed to several causes.

The section weighed included the accretion both above and below the extra two minutes of growth as well as the accretion both above and below the stagnation line,which was halved to give the value recorded in Table 4.4. As can be seen in Figures 2.1 and 2.2 the amount of ice below the stagnation line is greater than that above, for some of the runs. This is due to gravitational effects which are not included in the model. The section planimetered however was the half above the stagnation line, which would tend to underestimate the actual mass. Since the growth lines do not extend through the entire cross-section of the accretion for most runs, it was necessary to deduce the mass accreted per

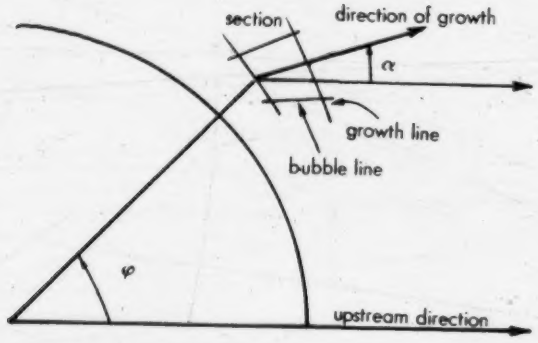

Figure 4.1. Schematic representation of angles deduced from bubble lines and growth lines. Section j at time t.

time step by assuming that the part of the accretion where growth lines were not present grew at the same rate as the part where they were present. The growth lines were then digitized, and the digitized data were used in subsequent calculations. The bubble lines and growth lines form a natural grid on the accretion dividing it into more or less rectangular sections. For each section two angles were measured. φ_{jt} represents the position of the section and is defined as the angle made by the free stream direction and the line joining the center of the cylinder to the center point of the trailing edge of the section (see Figure 4.1). The direction of growth α_{jt} is defined as the angle between the free stream direction and the line passing through the center of the trailing and leading edges of the section. This was done for each section and for every time step.

5. RESULTS

5.1 BUBBLE LINES

A most interesting result is one obtained from the behaviour of the bubble lines, described in Chapter 4. The data obtained from the analysis of the bubble and growth lines consisted of ρ_{jt}, the position angle at which the segment began, and α_{jt}, the direction of growth of the segment j at time t, the value of the elapsed time at the middle of the time step. All angles are in degrees. Only runs 2,3,4,7 and 9, were used in the following analysis, since the bubble lines in the remaining runs had insufficient clarity to warrant inclusion. Table 5.1 presents the results of a linear regression performed on ρ_{jt} and α_{jt}. For each accretion layer plots of these two angles against each other were seen to be approximately linear but they are not included here. For each regression, the value of the coefficient of determination, R, (King,1969) was found to be greater than .92. This lends credence to the visual observation of linearity.

Time(min)	1	3	5	7	9
Run #	$\varphi_{ot}/\frac{d\varphi}{d\alpha t}$	/	/	/	/
2	31/.73	30/.73	30/.80	33/.94	35/1.03
3	30/.93	33/.82	35/.70	34/.66	32/.62
4	37/1.22	36/1.02	34/.89	31/.72	31/.77
7	40/.72	38/.53	33/.49	32/.53	31/.58
9	39/.61	39/.52	38/.50	35/.52	32/.55
Average	35.4/.84	35.2/.72	34.2/.68	33.0/.67	32.0/.71

Table 5.1. Results of the linear regression of $\varphi_i t$ and $\alpha_i t$
φ_{ot} is the intercept of the regression.
$\frac{d\varphi}{d\alpha t}$ is the slope of the regression.

For each run φ_{ot} is the angle from stagnation at which forward growth ($\alpha=0$) occurs at time step t . These values are between 30 and 40 for all runs considered. Although it is not entirely valid to make a generalization using only the limited data given here, it is hoped that the results obtained for these five runs will be applicable to other similar runs. Although the scatter appears substantial it must be noted that a difference of only 10 degrees is in fact only 1/9 of the part of the cylinder under consideration. The values of φ_{ot} and $\frac{d\varphi}{d\alpha t}$ are therefore averaged to give the relations which are used in the model to define a direction of growth. The behaviour of $\overline{\varphi_{ot}}$ the average value, with time is linear (Figure 5.2) and follows the relation,

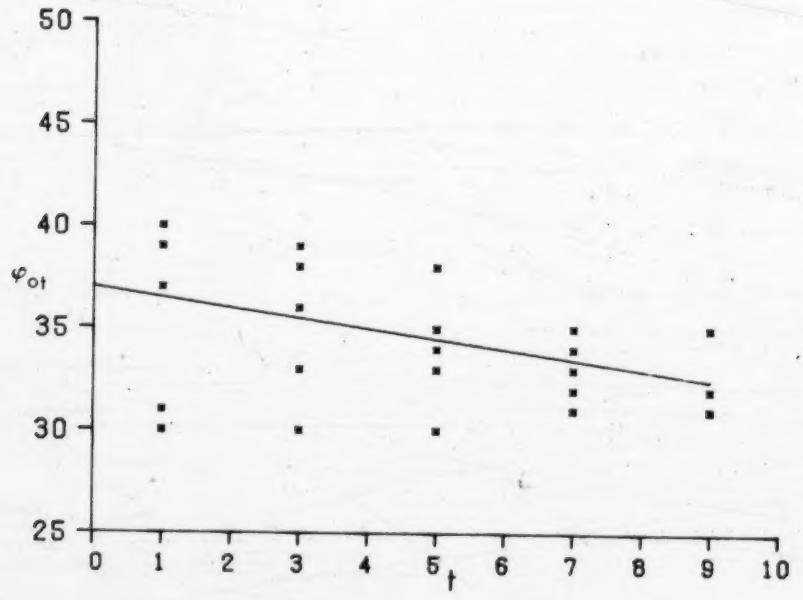

Figure 5.1. Intercept of regression φ_{ot} (degrees), t (min)

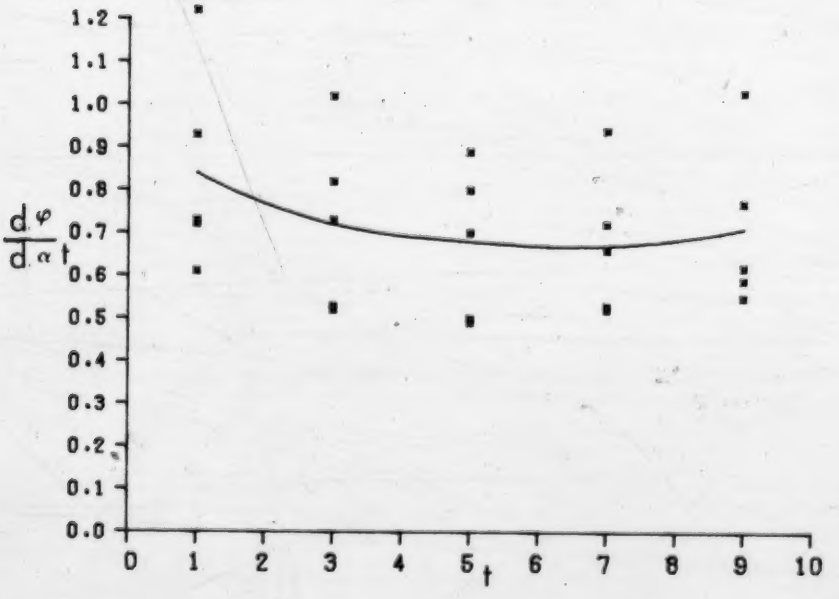

Figure 5.2. Slope of regression $\frac{d\varphi}{d\alpha t}$ (dimensionless), t (min).

$$\overline{\varphi_{or}} = 37 - \frac{t}{2} \qquad (5.1)$$

where t is the elapsed time in minutes from the start of growth.

The variation of $\frac{d\varphi}{d\alpha t}$ with time, though well behaved, is not linear and an interpolating polynomial (Newton Method) was used to give the relation,

$$\frac{d\varphi}{d\alpha t} = 7.81\times10^{-4}t^4 - 2.08\times10^{-3}t^3 + 2.42\times10^{-2}t^2 - 0.13t + 0.94 \qquad (5.2)$$

The quantity $\frac{d\varphi}{d\alpha t}$ is a measure of how much the segments diverge in the layer accreted during the time step centered on t, (see Figure 5.3). Equations 5.1 and 5.2 are used in the growth subroutine, described later in this chapter and listed in Appendix 6.

5.2 MASS

From the data obtained by planimetering the cross-sections, one can readily see that the mass growth rate is very nearly constant for each run. Figures 5.4 and 5.5 show cumulative mass accreted plotted against elapsed time for the -5°C runs and the -10°C runs respectively. Table 6.1 contains $\frac{dM_o}{dt}$ the slopes of the least squares regressions performed on M_o, the observed cumulative mass and t. That the coefficient of determination, R, is greater than .97 for all runs suggests that a linear representation is valid. The observed rate of growth, $\frac{dM_o}{dt}$,

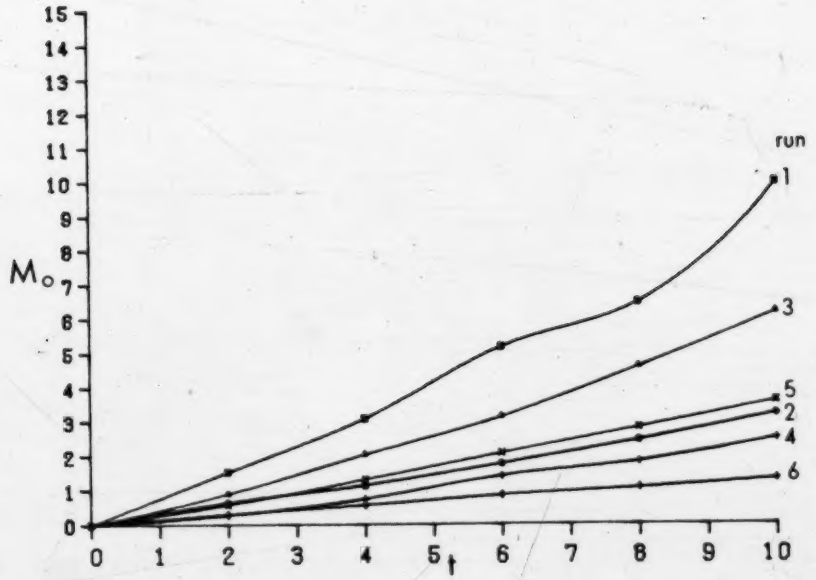

Figure 5.3 Runs at -5°C. Observed values.
Mass (g per cm along cylinder)
Time (minutes)

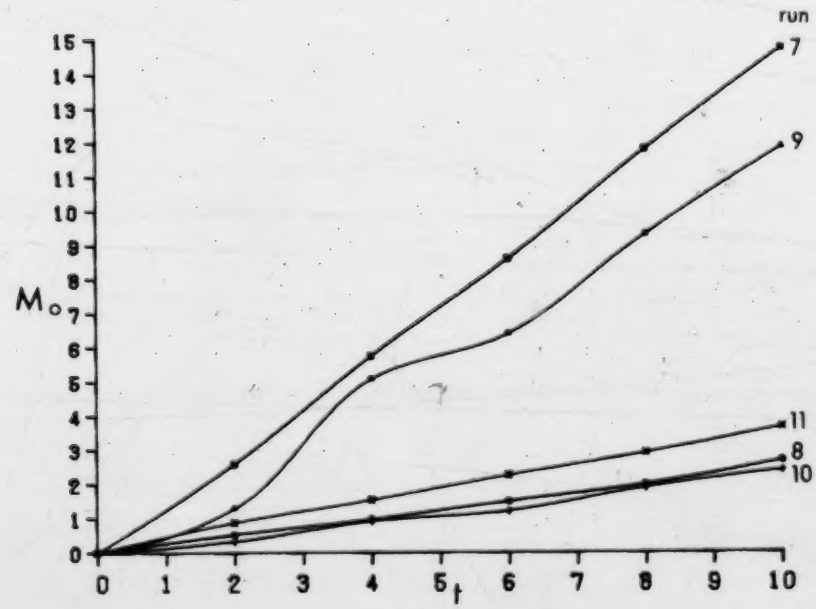

Figure 5.4 Runs at -10°C. Observed values.
Mass (g per cm along cylinder)
Time (minutes)

is plotted against the free stream flux, F_o , for each run in Figure 6.1. The relation, based on a linear regression is,

$$\frac{dM_o}{dt} = 2.40\, F_o \qquad (5.3)$$

The coefficient of determination for this regression is .98. The value for run 1 was excluded from the regression between the growth rate and flux, due to the uncertainty in the calculation of its LWC.

Since it is not immediately obvious that the accreted mass should increase linearly with time, a simple model may help to explain this result. For uniform accretion on the upstream half of a cylinder, with no shedding, the accretion rate is given by the relation (see Appendix 4),

$$\frac{dM_T}{dt} = a E_T + \frac{a^2 b E_T^2}{2}\, t \qquad (5.4)$$

In Appendix 4 it is also shown, by scale analysis, that the second term on the right hand side is an order of magnitude lower than the first for the time span considered here. Therefore in this simplified model the growth rate is essentially constant for each run, or in other words the mass increases linearly with time. Because this simplified model is not entirely unrealistic, a similar effect may be expected and is, indeed, observed in the actual behaviour.

5.3 SHAPE OF THE ACCRETION

Since the model provides an initial growth rate only, and the objective is to extrapolate this growth rate in time, a suitable procedure must be developed to do this. Towards this end two comparisons are made between the model and the experimental results. The first and simplest, used by Lozowski et al.(1979), involves the use of the initial growth rate given by the model, extrapolated linearly with time in a radial direction. The second also uses the linear extrapolation of the growth rate given by the model; however, the direction of growth is determined by the relations deduced from the bubble-line data, Equations 5.1 and 5.2. For this purpose a growth subroutine was added to the original model. A listing of this subroutine appears in Appendix 6.

The growth technique used in this subroutine is as follows. A diagrammatical representation is found in Figure 5.6. The assumption is made that the impinging water flux remains constant with time on the surface of the accretion for each sector regardless of the size of the accretion. Also, all functions of the angle around the cylinder described in Appendix 3 are assumed to remain constant with time and with the size of the accretion. This assumption has to be made for lack of information on how the changing shape affects the the angular distribution of the impinging flux. The ice is then allowed to grow in 30 second time steps for the "directional" procedure. This is deemed to be the

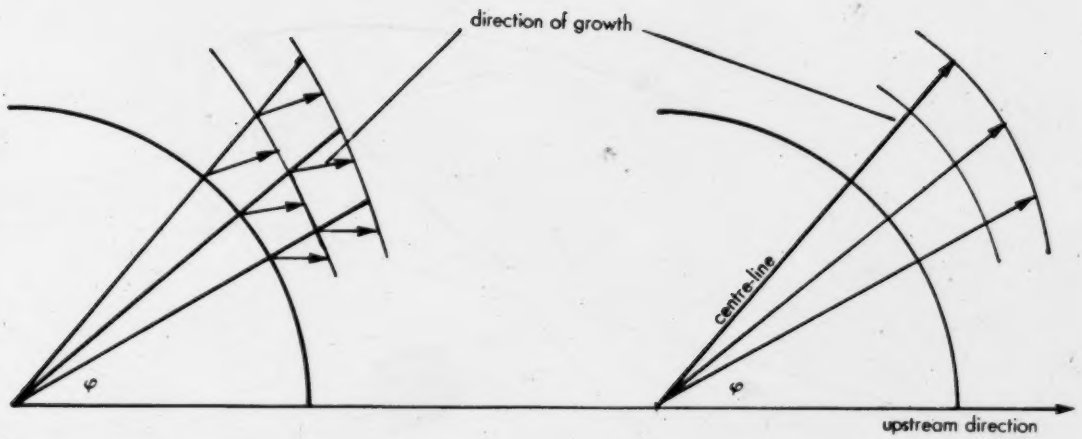

Figure 5.5. Method of interpolation for directional and radial growth technique.

minimum time step which allows enough ice to grow to avoid truncation errors in computation. It also gives a minimum growth per time step in Run 12 for example of 150μm. This is considered to be about the minimum value one should consider since it is the diameter of some of the larger droplets.

In the radial growth method the ice is allowed to grow radially outward in one time step of the same duration as the desired growth time, and at a rate governed by the initial growth rate calculated in the program. The directional growth technique also uses this growth rate over 30-second time steps, but the ice, rather than growing radially, grows in a direction governed by Equations 5.1 and 5.2. The new surface at the end of a particular time step is interpolated to give the points of intersection with the center lines of the sectors. These are the starting points of the growth for the next time step.

The validity of the assumption that the impinging water flux at each angle around the cylinder remains constant with time regardless of the overall size of the accretion was tested by allowing the cylinder to increase in diameter after each time step to a diameter corresponding to the original diameter plus the average thickness of the accretion at that time step. The new impingement fluxes were then calculated before proceeding with the next time step. This was found to give rise to a decrease in the ice thickness of only 2% in the worst case (run 7 after 10 minutes of growth) and so it can be ignored. Effects due to the change in shape of the accretion cannot be handled by the model since inclusion of these would require an understanding of the feedback between the airflow and the shape of the accretion. Oleskiw (1979, private communication), has already begun some work on this aspect of the problem.

Figures 5.6 through 5.17 give a visual comparison of the experimental results (upper outlines) with the theoretical results (lower outlines) using radial growth and directional growth. The corresponding graphs depict the angular distribution of the fraction of the experimental accretion predicted by the model after 10 minutes of growth. Because the results are not substantially different for growth times of less than 10 minutes these have been omitted for the sake of clarity. Figure 5.18 provides a comparison between forward growth, which is parrallel to the upstream

direction, and radial growth for run number 12. As suggested by Lozowski et al.(1979), forward growth gives reasonable results for dry growth cases and Run 12 was nearly dry. Run 1 must be treated with suspicion due to the apparent underestimation of the experimental value of the LWC.

The ratio $\frac{\tau_m}{\tau_o}$ represents the model-predicted thickness after 10 minutes of growth, divided by the observed thickness after 10 minutes of growth as a function of angle around the cylinder. Perfect agreement would occur if this were equal to unity at all angles, and agreement in shape only would occur if this were constant around the cylinder. The figures show the accretion only out to the angle at which the growth lines became indiscernible for that particular run, since a quantitative measurement of the time history of the accretion beyond this point is not possible. A discussion of these results is presented in Chapter 6.

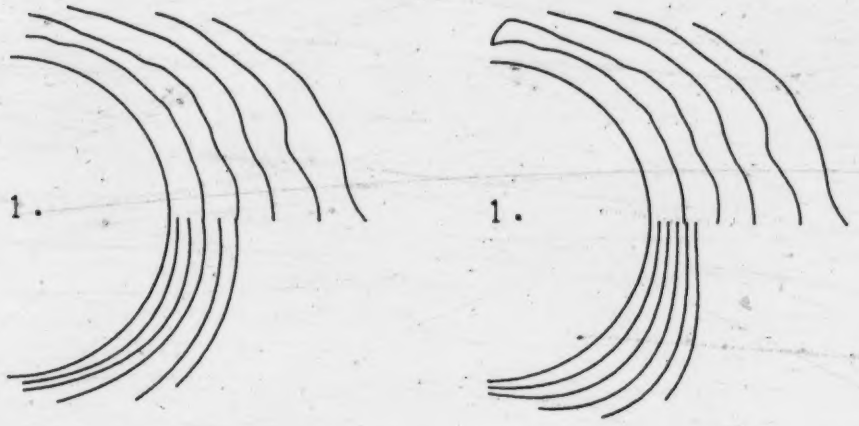

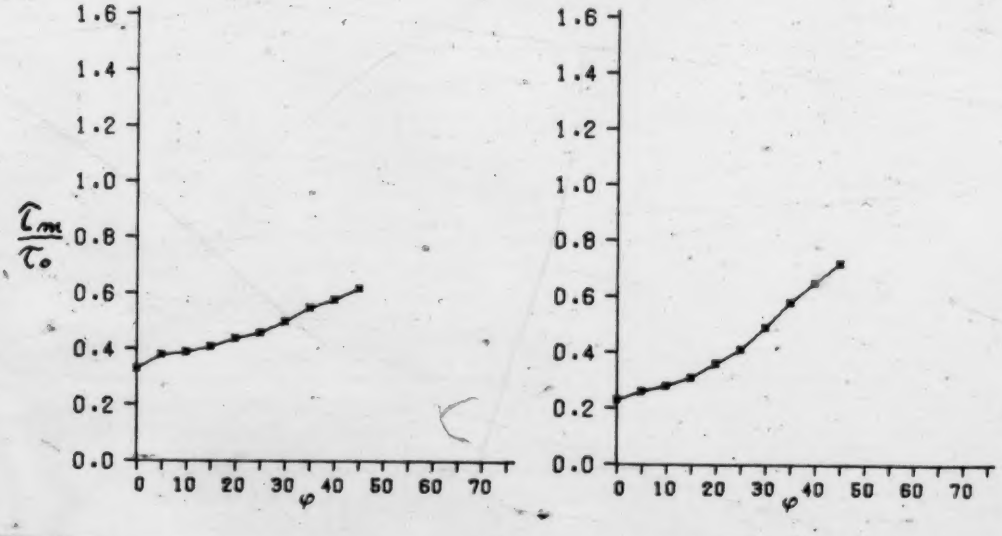

DIRECTIONAL RADIAL

RUN 1

T=-5°C V=45 m sec^{-1} LWC=1.79 g m^{-3}

Figure 5.6 Plots for growth lines, observed (upper lines) and predicted (lower lines).
Plot of ratio of measured to observed thickness $\frac{\tau_m}{\tau_o}$ versus angle around cylinder φ.

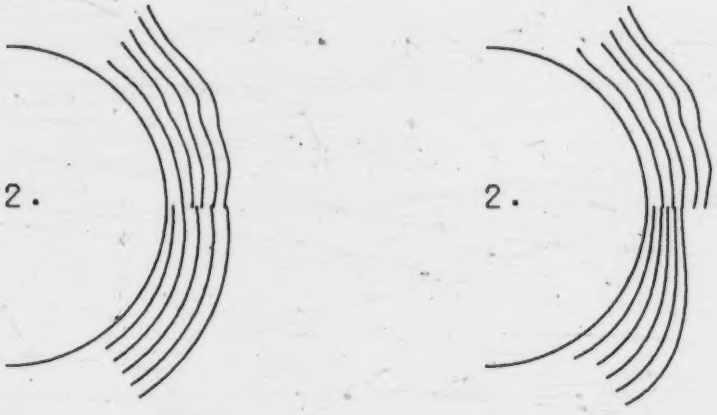

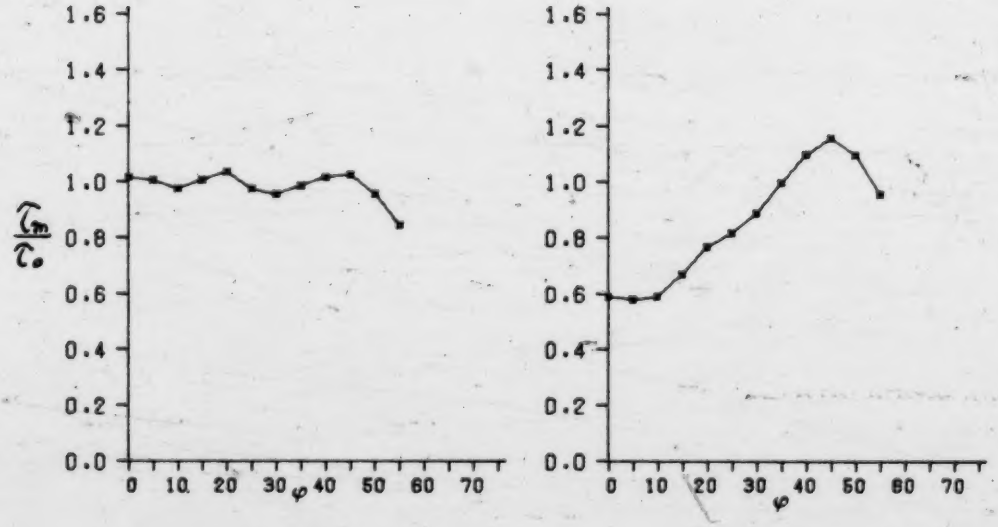

DIRECTIONAL RADIAL

RUN 2

T=-5 °C V=45 m sec^{-1} LWC= .80 g m^{-3}

Figure 5.7 Same as Figure 5.6

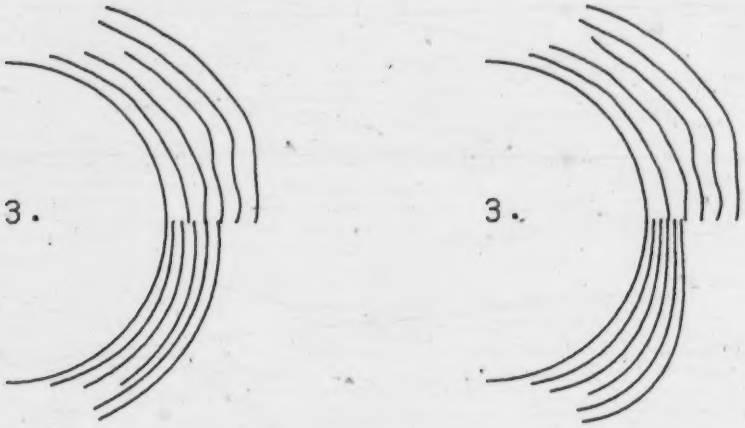

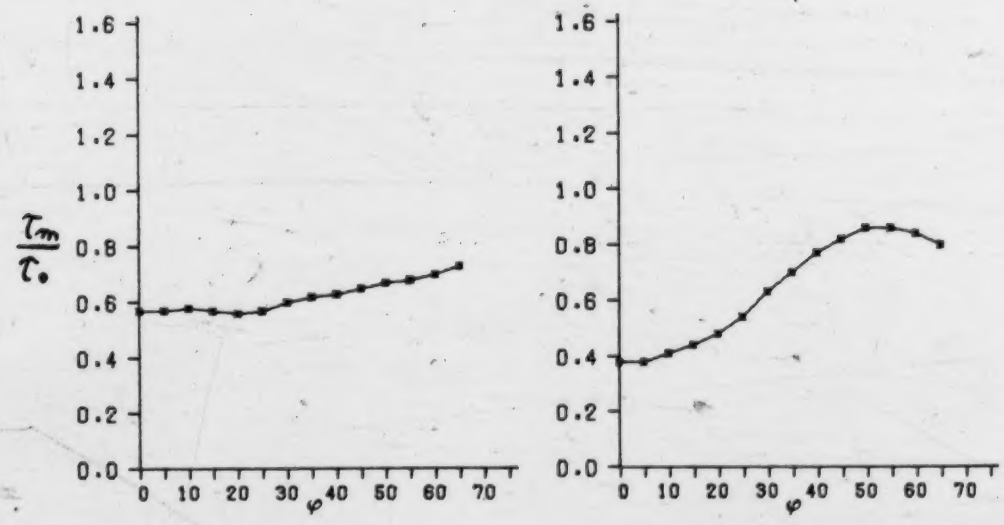

DIRECTIONAL RADIAL

RUN 3

T=-5°C V=30 m sec^{-1} LWC=1.54 g m^{-3}

Figure 5.8 Same as Figure 5.6

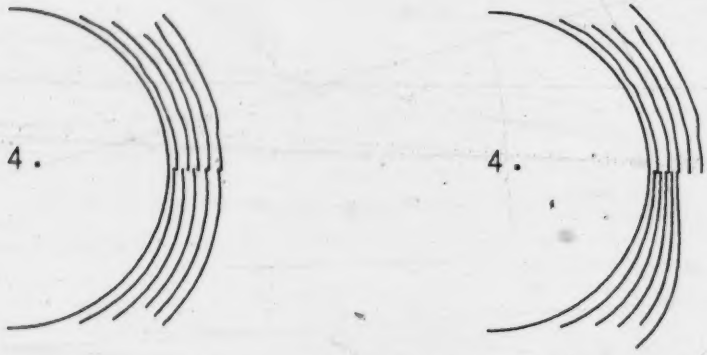

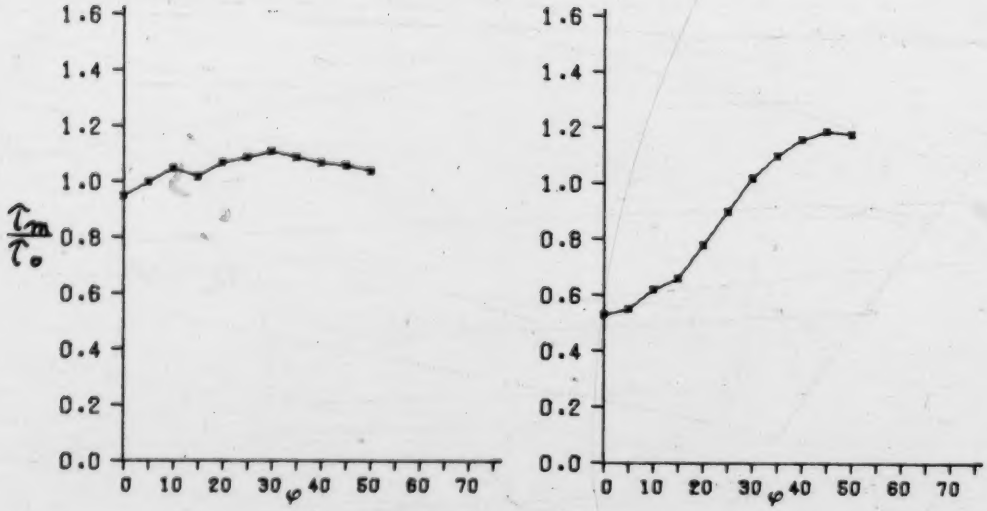

DIRECTIONAL RADIAL

RUN 4

T=-5°C V=30 m sec^{-1} LWC= .81 g m^{-3}

Figure 5.9 Same as Figure 5.6

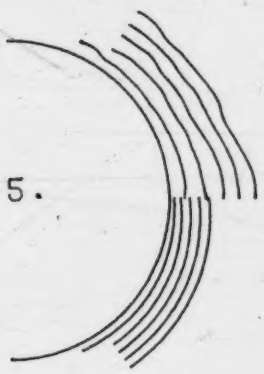

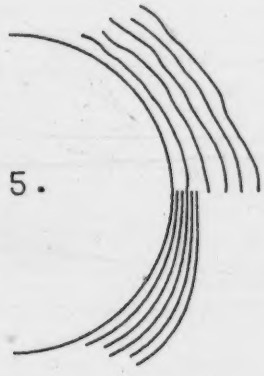

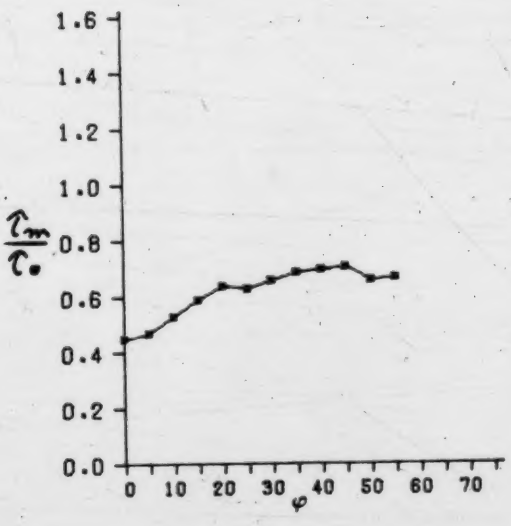

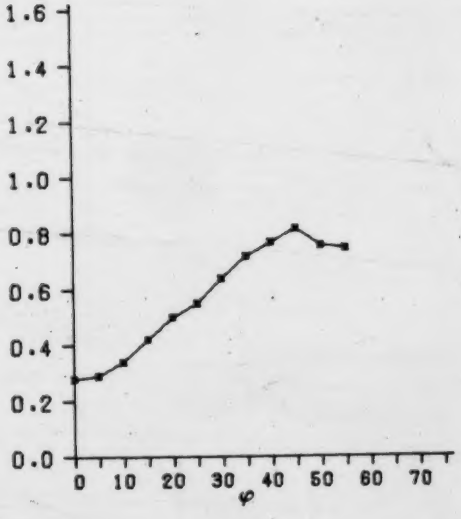

DIRECTIONAL RADIAL

RUN 5

T=-5°C V=15 m sec^{-1} LWC=2.04 g m^{-3}

Figure 5.10 Same as Figure 5.6

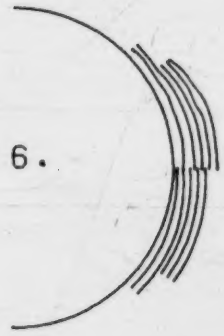

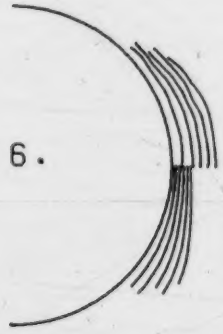

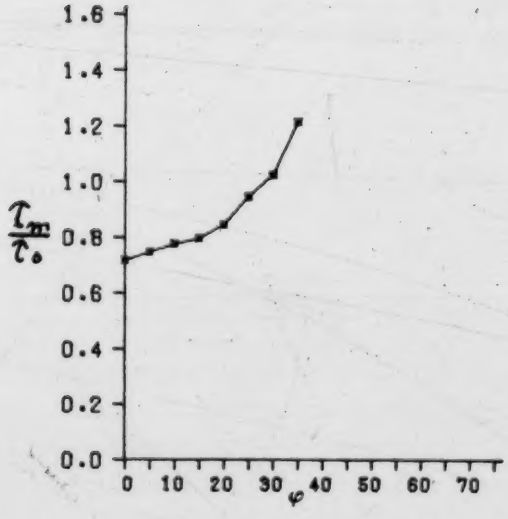

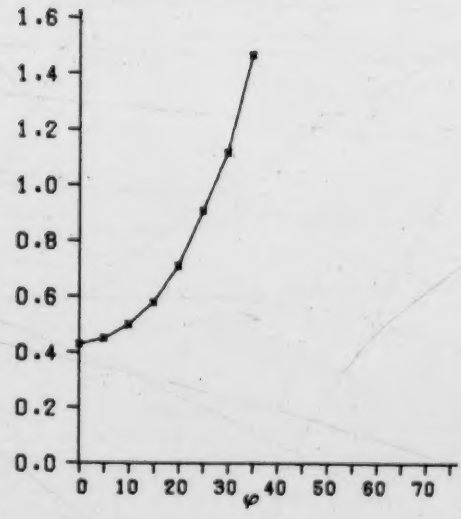

DIRECTIONAL RADIAL

RUN 6

T=-5 °C V=15 m sec^{-1} LWC= .75 g m^{-3}

Figure 5.11 Same as Figure 5.6

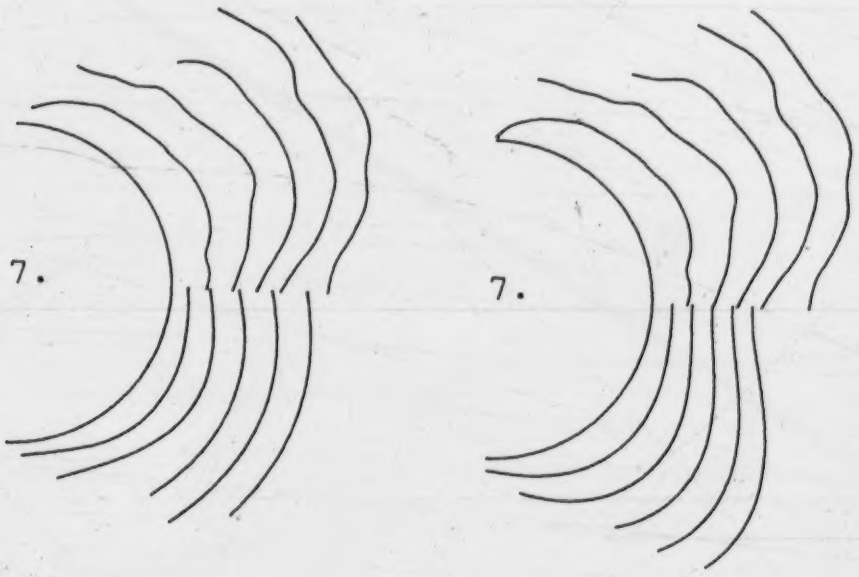

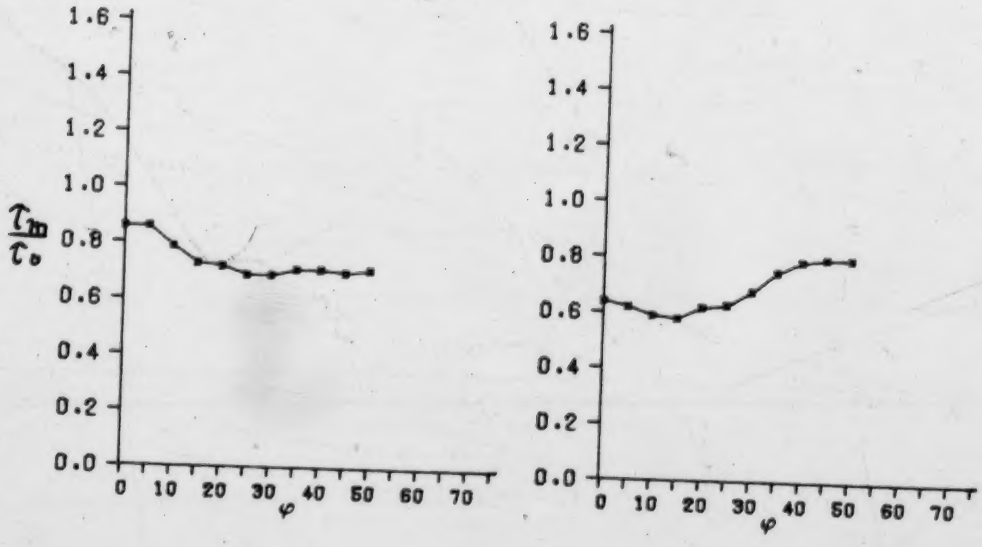

DIRECTIONAL RADIAL

RUN 7

T=-10 °C V=45 m sec^{-1} LWC=2.09 g m^{-3}

Figure 5.12 Same as Figure 5.6

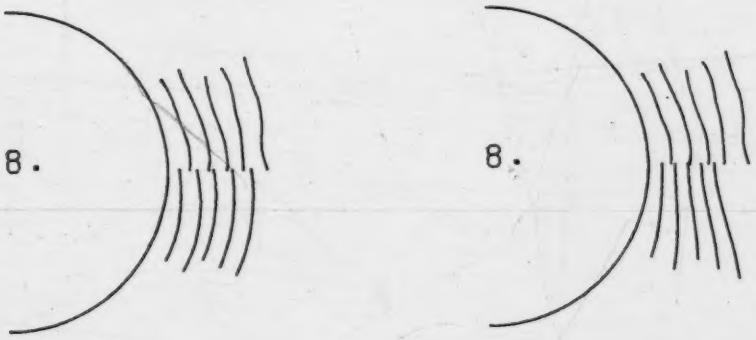

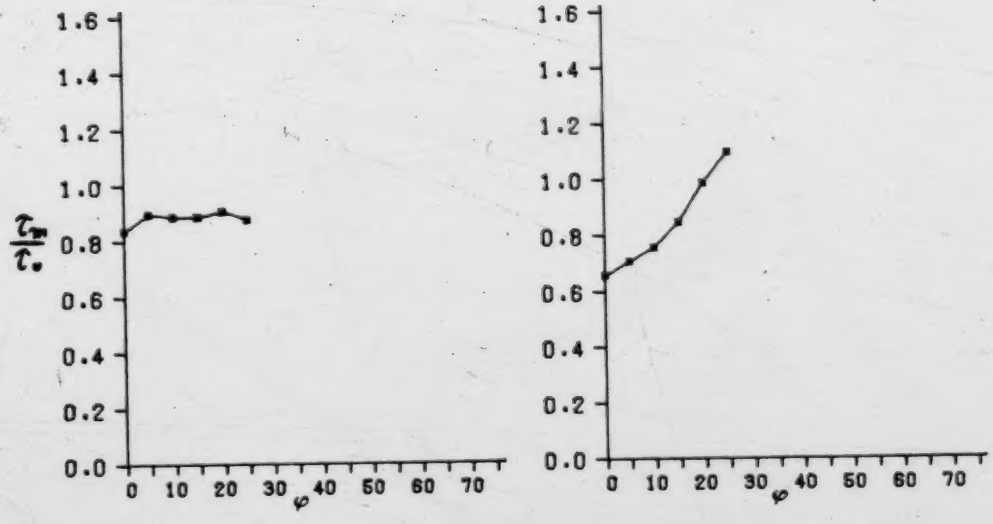

DIRECTIONAL RADIAL

RUN 8

T=-10°C V=45 m sec^{-1} LWC= .69 g m^{-3}

Figure 5.13 Same as Figure 5.6

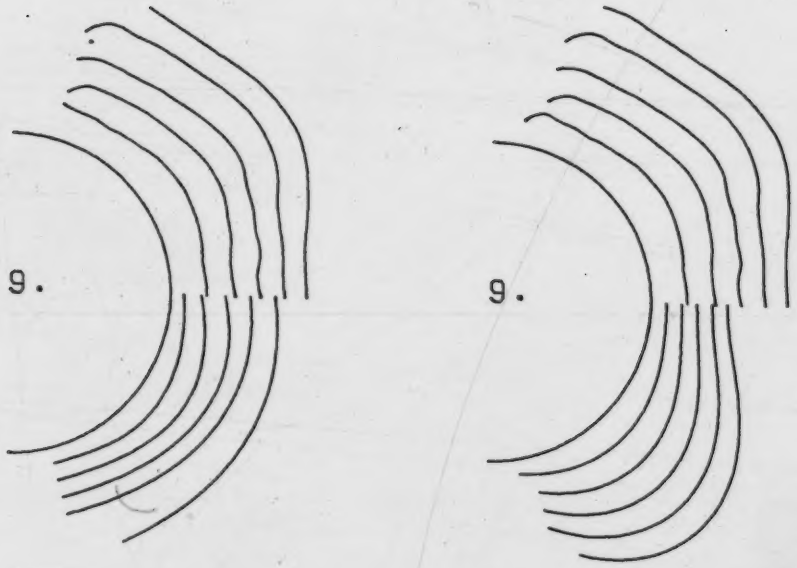

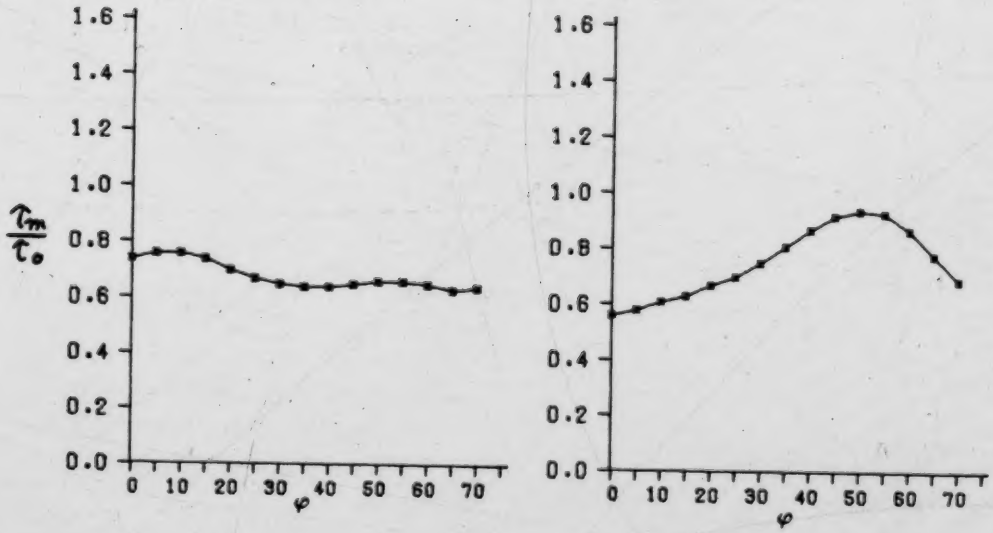

DIRECTIONAL RADIAL

RUN 9

T=-10 °C V=30 m sec^{-1} LWC=2.13 g m^{-3}

Figure 5.14 Same as Figure 5.6

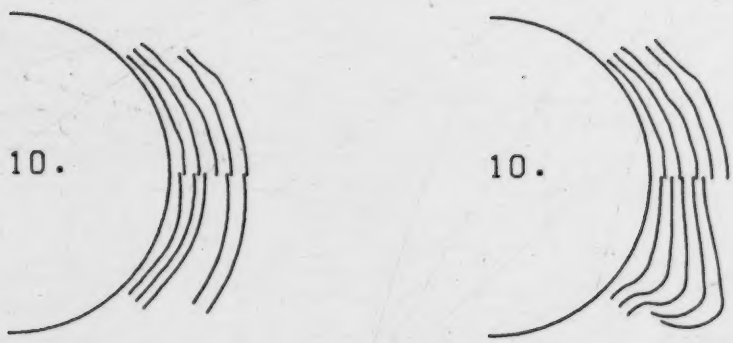

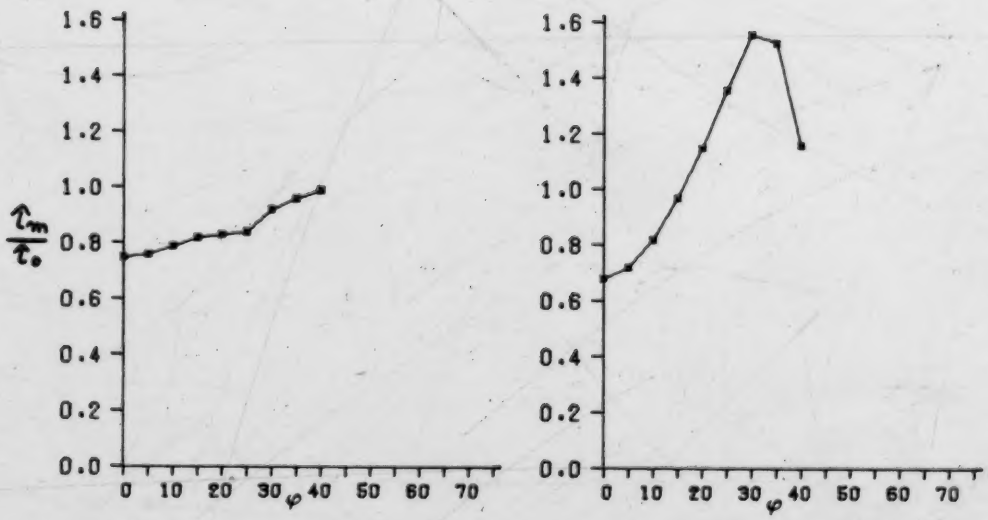

DIRECTIONAL RADIAL

RUN 10

T=-10 °C V=30 m sec^{-1} LWC= .69 g m^{-3}

Figure 5.15 Same as Figure 5.6

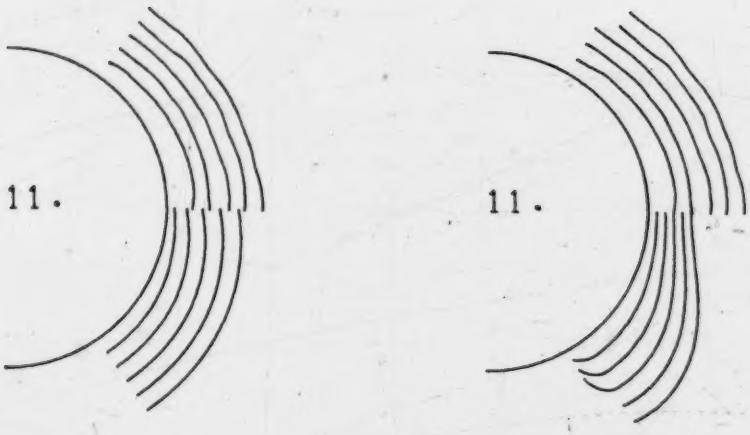

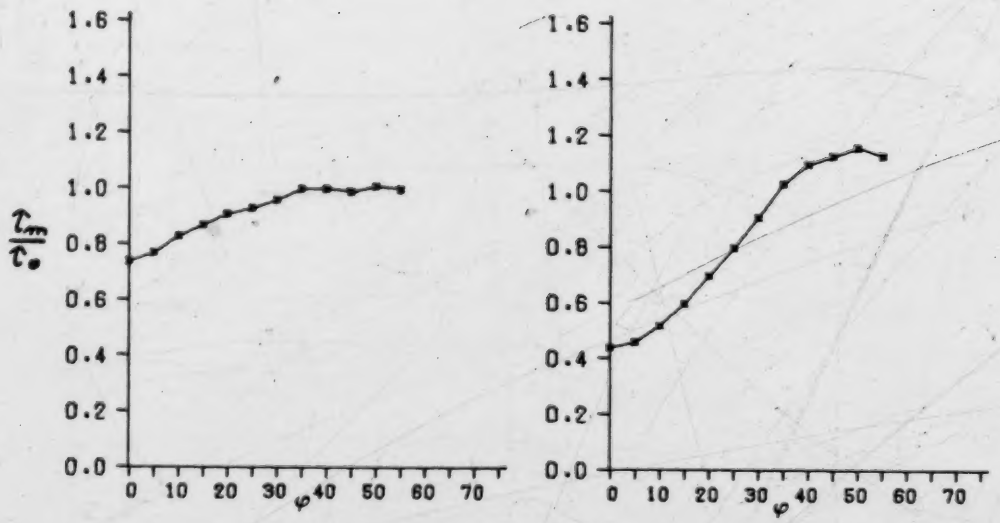

DIRECTIONAL RADIAL

RUN 11

T=-10 °C V=15 m sec^{-1} LWC=1.51 g m^{-3}

Figure 5.16 Same as Figure 5.6

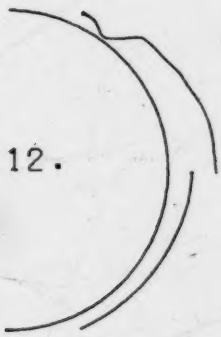

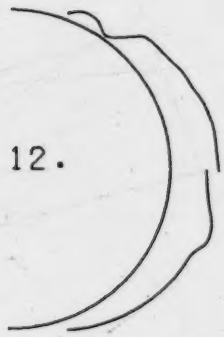

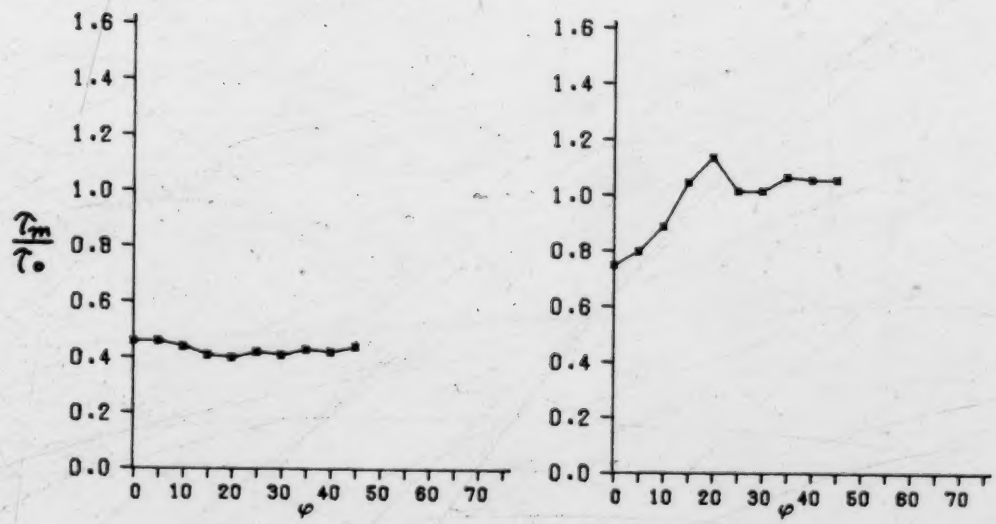

DIRECTIONAL RADIAL

RUN 12

T=-10 °C V=15 m sec^{-1} LWC= .73 g m^{-3}

Figure 5.17 Same as Figure 5.6

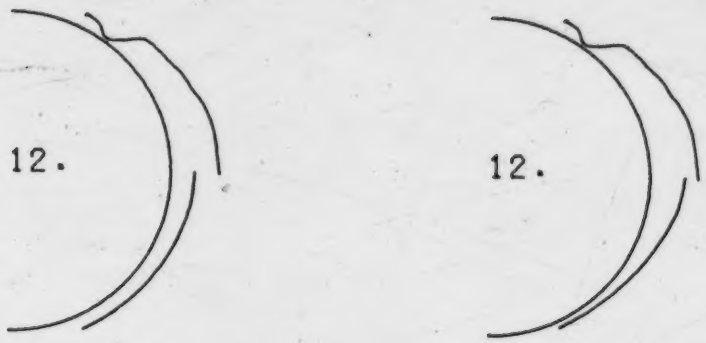

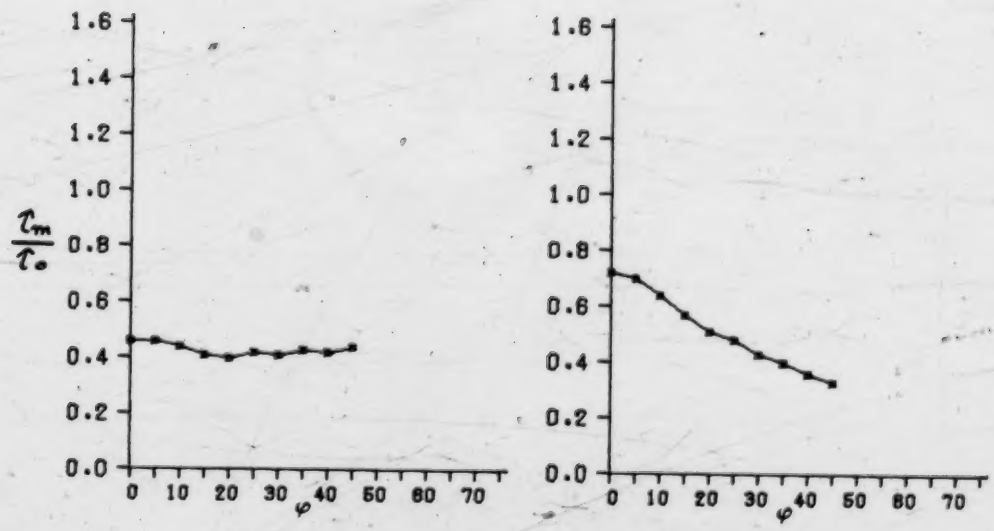

DIRECTIONAL FORWARD

RUN 12

T=-10 °C V=15 m sec^{-1} LWC= .73 g m^{-3}

Figure 5.18 Same as Figure 5.6

6. DISCUSSION

It is useful at this juncture to reiterate the objectives of this thesis before discussing the results presented in Chapter 5 in light of them. These are firstly, the prediction of mass of the accretion as a function of time and atmospheric conditions, and secondly the prediction of the shape of the accretion as a function of time and atmospheric conditions.

6.1 MASS PREDICTION

In Chapter 5 it was demonstrated that the observed mass of the accretions increased very nearly linearly with time for each run or, that the growth rate was a constant for each run independent of time, (Figures 5.4 and 5.5). From Figure 6.1, it is also reasonable to approximate the observed growth rate as a linear function of the free stream flux as given by Equation 5.3. Furthermore, as is demonstrated by Equation 5.4 and the discussion in Appendix 4, the simple model of uniform accretion does in fact predict a growth rate independent of time over the growth time under consideration (10 minutes). This theoretical growth rate is a function of the free stream flux F_o and the overall collection efficiency, E_T . F_o is a constant for a given run. Thus to the extent that the uniform accretion model simulates the actual mass growth behaviour, it would

Run #	E_T	E_m	E_{ms}	$\frac{dM_m}{dt}$	$\frac{dM_o}{dt}$
1	.80	.82	.28	.32	.90
2	.61	.85	.56	.28	.31
3	.90	.81	.39	.25	.58
4	.68	.77	.69	.24	.23
5	.82	.82	.43	.18	.35
6	.83	.78	.78	.13	.13
7	1.11	.84	.50	.67	1.46
8	.60	.81	.81	.37	.26
9	1.30	.82	.58	.52	1.16
10	.79	.80	.80	.24	.23
11	1.17	.78	.78	.26	.37
12	.72	.78	.78	.13	.11

Table 6.1. Overall collection efficiencies and growth rates
E_T uniform accretion collection efficiency
E_m Langmuir and Blodgett collection efficiency
E_{ms} accounts for shedding
$\frac{dM_m}{dt}$ model growth rate
$\frac{dM_o}{dt}$ observed growth rate

appear that any non-linearity in the relation between the growth rate and time is most likely due to the variation of E_T with time. Table 6.1 lists the values of E_T which would give the observed growth rate for each run using Equation 5.4, if the accretion were uniform. Also presented in this table is the overall collection efficiency E_m given by the model of Appendix 3, and this latter quantity reduced to take into account the water that the model predicts will be shed into the stream, E_{ms}.

In Table 6.1, some values of E_T are greater than one which is not consistent with the definition of collection efficiency. This however, is attributable to the method of

calculation of E_T and is consistent with the characteristics of the observed accretions. In the uniform accretion model the calculation of E_T does not fully take into account the increasing area presented to the free stream by the growing accretion and it is consequently an overestimation of the collection efficiency. For the larger accretions therefore, the use of the uniform accretion model will be expected to overpredict the overall collection efficiency at the first time step by a greater amount than it would for a smaller diameter accretion. This is undoubtedly the case for most of the runs and especially for runs 7 and 9.

Except for runs 7,9 and 11 the values of E_m are comparable to or less than E_T . This suggests that the initial overall collection efficiency predicted by the model does in fact allow for the presence of a sufficient amount of water on the cylinder, for the accretion to achieve the mass observed for that run. However, for the runs which grew entirely wet and had relatively small accretions (runs 1,2,3,4 and 5), the amount of water shed into the stream by the model was too large for the predicted growth rate to approach the observed. In fact when a comparison is made between the observed growth rates and the predicted growth rates as functions of the free stream flux, (Figure 6.1 and 6.2), it is apparent that on the whole the model of Appendix 3 underpredicts the growth rate by about 50%. The relation for the observed growth rate as a function of F_o is Equation 5.3, while that for the predicted growth rate is,

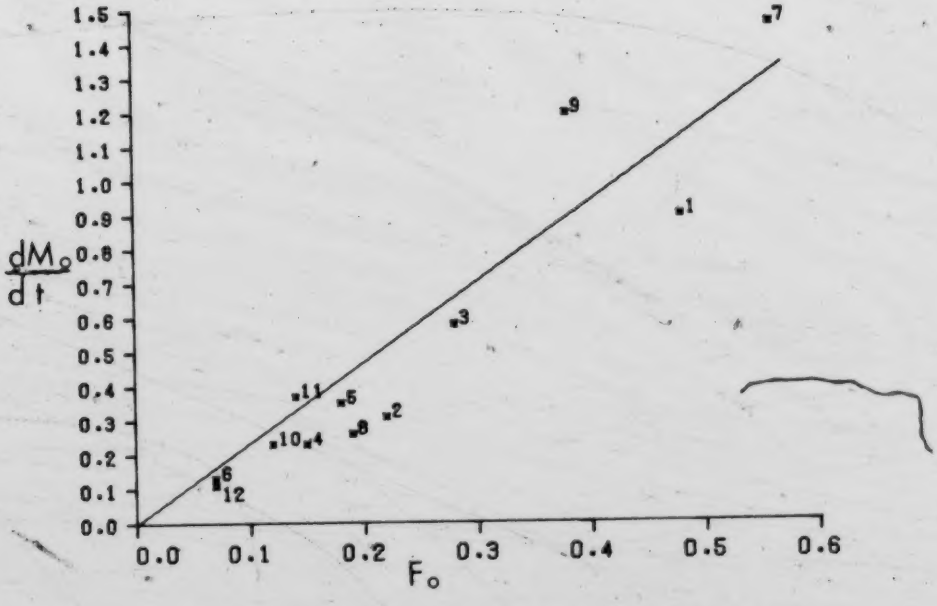

Figure 6.1 Observed growth rate ($g\ cm\ min^{-1}$)
versus free stream flux ($g\ cm^{-1}min^{-1}$)

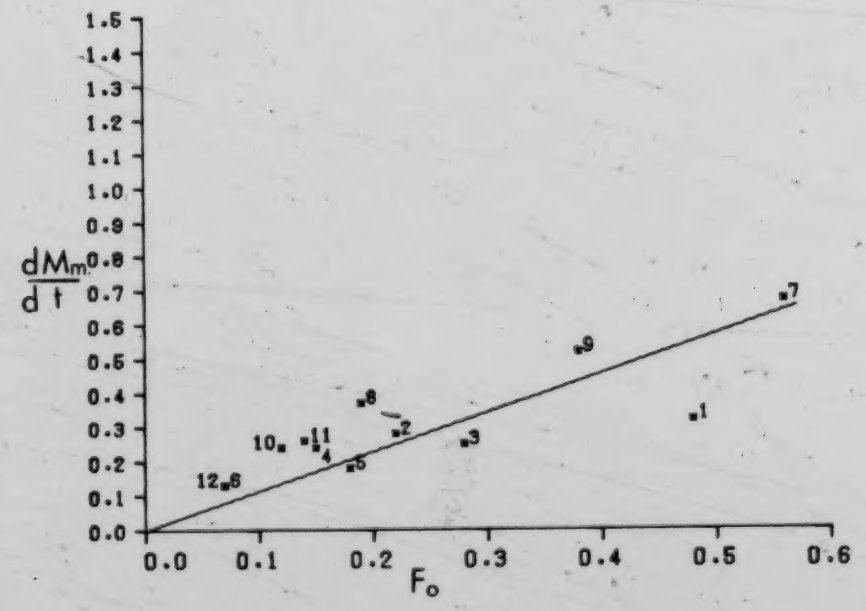

Figure 6.2 Model growth rate ($g\ cm\ min^{-1}$)
versus free stream flux ($g\ cm^{-1}min^{-1}$)

$$\frac{dM_m}{dt} = 1.14\,F. \qquad (6.1)$$

As a working hypothesis, one may speculate that this discrepancy between the observed and predicted relations is due to the presence of spongy ice. This is ice in which some or all of the water which the model predicts to be shed into the stream is in fact incorporated into the ice lattice and remains as part of the accretion. The model had no provision for this phenomenom to be included and therefore it only predicts at best the rate of "solid" ice accretion. Koos and Pum,(1974), suggest that the presence of protuberances on the surface of the ice accretion leads to the formation of spongy ice. In all runs, with the exception of number 12, protuberances were present and were in fact separated by the bubble lines discussed previously. The quantity of liquid water incorporated into the ice, as suggested by the findings of Gitlin and Goyer(1967) through calorimetric measurement of naturally occurring hailstones, may vary from about 2 to 16%. The difference between their findings and the apparent sponginess of about 50% which one can infer from Equations 5.3 and 6.1, may be attributable to a misrepresentation of the heat transfer characteristics in the model. This may arise from inadequacies in the theory of heat transfer used in the model. That is, if the actual heat transfer rate is higher than is used in the model, then more water would freeze and remain as solid ice. Since the model heat transfer is based on experimental values for a slightly

roughened cylinder, it is not surprising that it may underestimate the heat transfer for these very rough and non-cylindrical accretions.

6.2 SHAPE PREDICTION

Figures 5.6 through 5.17 present outlines of the observed growth for each time step (upper lines), and the model predicted growth for each time step (lower lines). Both the directional and radial methods of growth in the model are presented for each run as well as forward growth for run 12 in Figure 5.18. Below each representation of the cross-section is a graph of $\frac{r_m}{r_o}$, the ratio of the model-predicted thickness to the observed thickness at all angles around the cylinder out to the maximum angle for which growth lines were discernible.

In order to interpret the graphs of these figures, some general comments need to be made concerning them. A perfect fit to both the size and the shape of the accretion occurs when the values of this ratio are identically one for all angles. If the values of $\frac{r_m}{r_o}$ are constant for all angles but are not identically one, the shape of the predicted accretion is identical to the shape of the observed accretion although the size is not predicted accurately. The area under the curve is therefore proportional to the mass accreted up to the limiting angle of detectability of the growth lines.

Considering all the runs simultaneously it is possible to make the general observation that the directional growth technique gives accretions that more closely resemble the shape of the observed accretions than does the simple radial growth technique. This is apparent since the ratio $\frac{r_m}{r_o}$ for radial growth is not as consistent with angle as is the ratio for directional growth. There also is a tendency towards underprediction of size especially in the vicinity of the stagnation line, for most cases. Having made these observations the only curves considered from this point forward are those for directional growth.

Considering the -5°C, runs 1 through 6, it appears that the model predictions improve with increased wind speed, and that for a given wind speed the run with the lower LWC (even-numbered runs), is more accurately predicted than that with the higher LWC. In fact runs 2 and 4 are very nearly perfectly predicted if one disregards minor variations which are due to the irregularity of the surface of the observed accretion.

When considering the -10°C runs the problem of the "large" accretions, 7 and 9, is encountered. These runs are underpredicted by the model; however this is not, as in the other cases, most noticeable near the stagnation line of the cylinder. This is possibly due to the rather prominent hollow on the stagnation line which undoubtedly greatly affects the flow and renders less accurate the assumption of constant collection efficiency and growth rate. Runs 8,9 and

11, like the -5°C cases present an effectively cylindrical shape to the stream and behave in a similar fashion as the -5°C runs with respect to airspeed and LWC. It is pointed out in Chapter 5 that increasing the diameter of the cylinder by a small amount does not seriously affect the collection efficiencies and heat transfer rates calculated by the model. The accretion of run 12 appeared to grow dry. The directional growth technique gives a good representation of the shape for this case, as does the forward growth method, which also gives a better representation of the size.

Although it is not possible at this point and with these limited data to make a generalization, one can postulate that the difference in the shape between the observed and predicted accretions may be due to the presence of spongy ice in the observed accretions. Since the model does not include spongy ice growth, one would expect that it's accuracy would be better for "drier" cases. This is borne out by the observations that the predicted shape and mass is better for lower LWC and the same airspeed and temperature and for relatively higher airspeeds at similar LWC. Intuitively one would expect that lower LWC implies that relatively less water is available for incorporation as spongy ice at constant temperature and airspeed. Also a higher wind speed implies increased drag and consequently a thinner film on the surface of the accretion (Tenner and Blows,1976). This in turn should decrease the

sponginess if one considers that a thinner water film implies that less water is capable of being trapped in the ice as it forms.

It must be kept in mind also, that the heat transfer characteristics are undoubtedly affected by the size and shape of the accretion, however it is difficult to make a quantitative assessment of the behaviour of these characteristics at this point. One may only speculate that due to the presence of protuberances on the accretion, a drier growth regime would exist than the one described in the model.

7. CONCLUSION

The objective of this thesis was to extend the model of Lozowski et al.,(1979), to include time-dependence of the growth of ice on a non-rotating cylinder. The approach used was to evaluate the model and by the application of experimental results to extend the model to allow for time dependence of the growth of the accretion. Two criteria have been applied in order to assess the success of this endeavour. These are the ability to predict the mass of the accretion and the shape of the accretion.

In Chapters 5 and 6, relations were found which permitted the estimation of the mass growth rate from a knowledge of the free stream flux. Strictly speaking these relations are valid only for the temperatures, LWC, airspeed and cylinder size used in the experiment, although the applicability of the relation may extend outside this range. If one assumes that the model accurately predicts the amount of "solid" ice, the suggestion is that 50% of the actual accretion is liquid water for most of the runs considered. If this is in fact the case, the proper inclusion of spongy ice would no doubt improve the predictive properties of the model, as would a more accurate representation of the heat transfer characteristics associated with the changing roughness and shape of the accretion.

Further evidence has been assembled through the present

work to reinforce the interpretation of the bubble lines as indicators of the direction of growth of the lobes (Macklin,1977). The application of the data obtained from their analysis significantly improves the prediction of the shape of the accretion over the radial growth assumption.

The use of the shield technique to delineate the shape of the ice at a given time worked very well indeed. Whether or not it greatly affects the growth of the accretion is not known and a better understanding of why ice grows clear or opaque should lead to some indication of its actual effect. The transition to a new steady state with insertion and removal of the shield is in all probability quite rapid and it appears that the effect of the shield on the accretion would be minimal.

In summary then, the approach of using a theoretical model complemented by experimental observation is a viable method of improving the prediction of icing on a cylinder.

Suggestions for future work include,

a. The theoretical or experimental consideration of the effect of the changing accretion shape on the flow, collection efficiency and heat transfer.

b. Theoretical or experimental consideration of the thermodynamics and mechanics of the formation of spongy ice.

c. Collection of more data over a wider range of conditions to develop empirical relations between the parameters of ice accretion and the size and

shape of the accretion.

d. Concentration on the variation of one parameter in particular. Most fruitful would be concentration on wind speed due to the inherent uncertainty in present methods for the measurement of LWC.

e. Improvement of tunnel controls to give more stable and reproducible atmospheric conditions.

f. An extension to an airfoil for the problem of helicopter icing is a logical step when considering the effect of a non-cylindrical shape.

References

Ashworth, E., T. Ashworth, C. A. Knight, 1978: Analysis parameters for accreted ice. Preprints of the Conference on Cloud Physics and Atmospheric Electricity, Issaquah Wash. U.S.A., July-Aug, 86-193.

Ashworth T. and C. A. Knight, 1978: Cylindrical ice accretions as simulations of hail growth, Part 1. Journal of the Atmospheric Sciences, 10, 1987-1996.

Ashworth T. and N. Knight, 1978a: Cylindrical ice accretions as simulations of hail growth Part 2. Journal of the Atmospheric Science, 10, 1997-2009.

Carras J.N., S. Thwaites and W.C. Macklin, 1977: The aerodynamics of oblate hailstones. Quarterly Journal of the Royal Meteorological Society, 103, 803-808.

Carte A.E., 1961: Air bubbles in ice. Proceedings of the Physical Society, 77, 757-763.

Gitlin S.N. and G.G. Goyer, 1968: The liquid water content of hailstones. Journal of the Atmospheric Sciences, 25, 97-99.

King L.J., 1969: Statistical analysis in Geography, Prentice Hall, Englewood Cliffs N.J. U.S.A., 288 pp.

Langmuir, I. and K.B. Blodgett, 1961: A mathematical investigation of water drop trajectories. The collected works of Irving Langmuir, 10 , Pergamon Press, 1961, 335-393.

Lozowski, E.P., J.R. Stallabrass and P.F. Hearty, 1979: The icing of an unheated non-rotating cylinder in liquid water droplet-ice crystal clouds. National Research Council Canada, Division of Mechanical Engineering, Laboratory Technical Report LTR-LT-96.

Ludlam F.H., 1951: The heat economy of a rimed cylinder. Quarterly Journal of the Royal Meteorological Society, 77, 663-666.

Macklin W.C., 1975: Air bubbles in accreted ice. Quarterly Journal of the Royal Meteorological Society. 101, 127-146.

Macklin W.C., 1977: Characteristics of naturally occuring hailstones and their interpretation. Meteorological Monographs, 16 , 64pp.

Poots and Rodgers, 1975: Icing of a cable. Journal of the Institute of Mathematics and its Applications, 18, 203-214.

Rogers R.R., 1976: A Short Course in Cloud Physics. Pergamon Press, Oxford England, 227 pp.

Roos, D.S. and H.D.R. Pum, 1974: Sponginess in ice grown by accretion. Quarterly Journal of the Royal Meteorological Society. 100, 640-657.

Sroka M., 1972: Design of an atmospheric icing tunnel. Unpublished Master's Thesis, University of Alberta, Dept. of Mechanical Engineering, 74 pp.

Stallabrass, J.R., 1958: Canadian research in the field of helicopter icing. The Journal of the Helicopter Association of Great Britain, 12, 40 pp.

Seban, R.A., 1960: The influence of free stream turbulence on the local heat transfer from cylinders. Journal of Heat Transfer, 82, 101-107.

Stallabrass, J.R., 1978: An appraisal of the single rotating cylinder method of liquid water content measurement. National Research Council Canada, Dept. of Mechanical Engineering, Laboratory Technical Report LTR-LT-92.

Tenner, L.H. and L.G. Blows, 1976: A study of the motion of oil films on surfaces in air flow, with application to the measurement of skin friction. Journal of Physics E, 9, 194-210.

Zukauskas, A., 1972: Heat transfer from tubes in crossflow. Advances in Heat Transfer. 8, 93-160.

Appendix 1

This appendix contains the definitions of the variables used in the body and appendices of this thesis.

D_0 test cylinder diameter (m).

d_0 rotating cylinder diameter (m).

d_c diameter of ice accreted on rotating cylinder (m).

d_k mean diameter of droplets in k th category (m).

E_k overall collection efficiency for droplets in k th category.

E_m overall collection efficiency calculated by model.

E_{ms} overall collection efficiency accounting for shed water calculated by model.

E_T overall collection efficiency assuming uniform accretion.

F_0 free stream flux ($g\ cm^{-2} min^{-1}$).

F_R water flux into a sector from the upstream sector ($kg\ m^{-2} sec^{-1}$).

F_w water flux into a sector directly from the stream ($kg\ m^{-2} sec^{-1}$).

h heat transfer coefficient.

h_0 average heat transfer coefficient.

k_a thermal conductivity of air ($J\ m^{-1}$).

K_k inertia parameter for droplets in k th category.

K_{0k} non-dimensional inertia parameter for droplets in k th category.

LWC liquid water content of the air (kg m^{-3}).

ℓ length of rotating cylinder (m).

M_m mass per cm along cylinder predicted by model (g cm^{-1})

M_o mass per cm along cylinder as observed from planimeter measurements (g cm^{-1}).

M_T mass per cm along cylinder predicted by uniform accretion assumption (g cm^{-1}).

m mass of the ice on the rotating cylinder (kg).

N_u Nusselt number.

n freezing fraction of total water available in a sector.

P static pressure at stagnation line of bare cylinder (Pa).

P_o ambient air pressure (Pa).

ΔP pressure difference in inches of water for airspeed calculation (Pa).

R_{ec} Reynold's number of the test cylinder.

R_{ek} Reynold's number of the droplets in the k th category.

R_i accretion rate of ice (kg $m^{-2}sec^{-1}$) or (mm sec^{-1}).

π_t contraction ratio of tunnel. cross-sectional area of settling chamber divide by the cross-sectional are of the working section. (16).

S_c Schmidt number (0.595).

T_a ambient air temperature (°C).

T_s deposit temperature on surface of accretion (°C).

t time.

V relative velocity of free stream to test cylinder (m sec^{-1}).

α_{jt} direction of growth from bubble line calculations, of section j, at time t, (degrees). Measured from the upstream direction a positive value indicates divergence from the stagnation line of the cylinder.

β_j collection efficiency for sector j for all droplets.

β_{ok} stagnation line collection efficiency for droplets in the k th category.

ϵ ratio of molecular weight of water to the mean molecular weight of air (0.622).

φ_{jt} angular displacement from upstream direction of section j, at time t, for bubble line data (degrees).

φ angular displacement from upstream direction of centre-line of sector (degrees).

φ_{mk} maximum impingement angle on cylinder for droplets in the k th category (degrees).

λ actual ballistic range of a droplet (m).

λ_s Stoke's law ballistic range of a droplet (m).

μ_a dynamic viscosity of air (kg $m^{-1}sec^{-1}$).

ρ_a density of dry air (kg m^{-3}).

ρ_i density of ice (890 kg m^{-3}).

ρ_w density of water (1000 kg m^{-3}).

$\frac{\tau_m}{\tau_o}$ ratio of predicted to observed accretion thickness.

Appendix 2

This appendix contains a derivation of the formula used to calculate the LWC by the rotating cylinder method. The collection efficiency is assumed to be unity, since for very small objects it is very nearly unity and no quantitative measure could be made to find the actual value. Stallabrass,(1978) suggests a value of somewhat less than one which if valid implies that the measurements made using the formula derived here may be an underestimation of the LWC by about 10%.

Let

d_c be the outside diameter of the ice accreted

d_o be the diameter of the bare cylinder (2.79×10^{-3} m)

l be the length of the cylinder (3.75×10^{-2} m)

V be the free stream speed (m sec^{-1})

m be the mass of ice accreted (kg)

t be the time of exposure in the stream (sec)

ρ_i be the density of ice (890 kg m^{-3})

LWC be the liquid water content (kg m^{-3})

The volume swept out in time dt is $dV = d_c l V dt$

and hence the mass swept out is $dm = d_c l V LWC\, dt$ (1)

but $$m = \pi l \rho_i \left(\frac{d_c^2}{4} - \frac{d_o^2}{4} \right)$$

or $$d_c = \left(\frac{4m}{\pi l \rho_i} - d_o^2 \right)^{1/2} \quad (2)$$

Combinining 1 and 2 gives

$$\left(\frac{4m}{\pi \ell \rho_i} - d_o^2\right)^{-1/2} dm = V L W C \, dt \qquad (3)$$

Integrating

$$\int_0^m \left(\frac{4m}{\pi \ell \rho_i} - d_o^2\right)^{-1/2} dm = \int_0^t V L W C \, dt$$

results in

$$L W C = \frac{\pi \rho_i}{2 V t} \left\{\left(\frac{4m}{\pi \ell \rho_i} - d_o^2\right)^{\frac{1}{2}} - d_o\right\}$$

Appendix 3

A brief description of the calculations performed in the model follows. A complete description is found in Lozowski et al.(1979).

All variables are defined in Appendix 1.

Calculations performed in the program in chronological order are:

1. The calculation of parameters which are a function of the air temperature (T_a), and the Wind speed (V).

   dynamic viscosity of air; $\mu_a = 1.718\times10^{-5} + 5.1\times10^{-8} T_a$

   density of dry air; $\rho_a = \dfrac{P_o}{R_d(T_a + 273.16)}$

   thermal conductivity of dry air; $k_a = 2.43\times10^{-2} + 7.3\times10^{-5} T_a$

   Reynold's Number of the Cylinder; $Rec = \dfrac{V D_o \rho_a}{\mu_a}$

2. The calculation of parameters which are a function of droplet size of category (k), (Langmuir and Blodgett, 1961).

   Reynold's number of the droplets; $Rek = \dfrac{V d_k \rho_a}{\mu_a}$

   Non-dimensional inertia parameter; $K_{0k} = .125 + (K_k - .125)\dfrac{\lambda}{\lambda_s}$

   λ and λ_s are the actual and Stoke's law ballistic ranges respectively.

   and

$$K_k = \frac{\rho_w V d_k^2}{9 \mu_a D_o}$$

The non-dimensional inertia parameter thus defined accounts for the departure from Stoke's Law due to the velocities under consideration.

The ratio $\dfrac{\lambda}{\lambda_s} = (1 + 0.967\, Re_k^{.6367})^{-1}$ gives an empirical fit to the Langmuir and Blodgett (1946) data.

For different values of K_{oh} the parameters:

β_{oh}, Stagnation line collection efficiency

E_h, Overall collection efficiency

φ_{mh}, Maximum impingement angle

are determined as follows:

$K_{oh} < .125$ $\qquad \beta_{oh} = E_h = \varphi_{mh} = 0$

$.125 \leq K_{oh} < 7.5$ $\qquad \beta_{oh} = \dfrac{1.4(K_{oh} - .125)^{.84}}{1 + 1.4(K_{oh} - .125)^{.84}}$

$7.5 \leq K_{oh}$ $\qquad \beta_{oh} = \dfrac{K_{oh}}{1 + K_{oh}}$ *

$.125 \leq K_{oh} < .9$ $\qquad E_h = .489(\log_{10} 8K_{oh})^{1.978}$ *

$.9 \leq K_{oh}$ $\qquad E_h = \dfrac{K_{oh}}{\frac{\pi}{2} + K_{oh}}$ *

$.125 \leq K_{oh} < 10$ $\qquad \varphi_{mh} = \tan^{-1}\{1.7(K_{oh} - .125)^{.96}\}$

$10 \leq K_{oh}$ $\qquad \varphi_{mh} = \tan^{-1} K_{oh}$

* Note that these equations have been modified to better fit the Langmuir and Blodgett numerical data.

3. The following calculations are performed for each sector (φ_j)
where φ_j is given by $\Delta\varphi(j-1); j=1,(\frac{90}{\Delta\varphi}+1)$.
For smooth surface assumption, the Nusselt Number is given by:

$$Nu = Re_c^{1/2}\left\{1-\left(\frac{2\varphi}{\pi}\right)^3\right\}$$

For rough surface assumption, the Nussault Number is given by:

$$Nu = Re_c^{1/2}\left\{2.4 + 1.2\sin(3.6\{\varphi-25°\})\right\}$$

The recovery factor after Seban(1960) is given by:

$$r_c = .75 + .25\cos 2\varphi$$

For each drop size the variation of collection efficiency with angle is given by Lozowski et al. (1979) as:

$$\beta_{jk} = \beta_{ok}\cos\left(\frac{\pi\varphi_j}{2\varphi_{mk}}\right) + \frac{\pi^3}{\varphi_{mk}^3(\pi^2-4)}\left\{\frac{E_k - 2\varphi_{mk}\beta_{ok}}{\pi}\right\}\left\{\varphi_j^2\sin\left(\frac{\pi\varphi_j}{\varphi_{mk}}\right)\right\};\ \varphi_j < \varphi_{mk}$$

Therefore, the collection efficiency for each sector (β_j) is found by summing the collection efficiencies of all droplet size categories for that sector,

$$\beta_j = \sum_k \beta_{jk}$$

The flux of supercooled water into the sector directly from the stream is then given by,

$$F_w = \sum_k f_k \beta_{jk}$$

where f_j is the fraction of the total mass flux in the undisturbed flow consisting of drops in the k th category.

4. Next the Ludlam limit for a rotating cylinder is calculated if required, according to a procedure originally given by Ludlam(1951).

For $Re_c \leq 2\times10^5$ the mean heat transfer coefficient is given by,

$$h_o = 0.229\frac{k_a}{D_o}Re_c^{.6}$$

For $Re_c > 2\times10^5$ the mean heat transfer coefficient is

given by,

$$h_o = 0.067 \frac{k_a}{D_o} Re_c^{.7}$$

The critical liquid water content (Ludlam limit) is given by,

$$LWC_{crit} = \frac{1}{F_\omega}\left\{-\pi h_o\left(T_a + \{\ell_s(T_a) - \ell_s(0^\circ)\}\frac{\ell_{a_p}\epsilon}{P c_p}\left(\frac{P_r}{S_c}\right)^{.63} + \frac{.4V^2}{2c_p(.5V^2 + 3.34\times10^5 c_\omega T_a)}\right\}\right.$$

5. The local static pressure for the evaporative cooling term used in the heat balance equation is given by

$$P = P_o + \{1.3\cos 2\varphi_i - .3\}\frac{\rho_a V^2}{2}$$

6. The heat balance equation is then solved by Newton's method. The heat balance equation in detail is:

$$h(T_a - T_s) + h\left(\frac{P_r}{S_c}\right)^{.63}\frac{\epsilon \ell_v}{P_{a_p}}\{\ell_s(T_a) - \ell_s(T_s)\} + F_\omega \bar{c}_\omega (T_a - T_s) + \eta F_\omega \ell_f(T_s) + \ldots$$

$$\ldots F_r \bar{c}_\omega (T_s^* - T_s) + \eta F_r \ell_f(T_s) + \frac{1}{2}\frac{h\pi_s}{c_p}U^2 + \frac{1}{2}F_\omega U^2 = 0$$

This equation has two unknowns the freezing fraction η and T_s. These are not independent and are related in the following manner,

$$T_s < 0 \text{ for } \eta = 1 \text{ and } T_s = 0 \text{ for } \eta < 1$$

Appendix 4

In this appendix a theoretical growth equation is developed assuming uniform accretion on the front half of a cylinder with no shedding. The accretion would appear as one half of an annulus.

The variables used in this development are defined in Appendix 1.

The rate of mass accretion on an obstruction which presents an area $D_o \ell$ to the stream is,

$$\frac{dM_T}{dt} = V L W C D_o E_T$$

for $\ell = 1$ cm

For one half of a cylinder the change in volume with time is given by,

$$\frac{dV}{dt} = \frac{\pi D}{2} \frac{dD}{dt}$$

Therefore,

$$\frac{dM_T}{dt} = \frac{\rho_i \pi D}{4} \frac{dD}{dt}$$

but,

$$D = \left(\frac{8 M_T}{\pi \rho_i} + D_o^2 \right)^{1/2}$$

so that

$$\frac{dM_T}{dt} = V L W C D_o E_T \left(\frac{8 M_T}{\pi \rho_i D_o^2} + 1 \right)^{1/2}$$

or $$\frac{dM_T}{dt} = aE_T(1+bM)^{1/2}$$

where $a = V LWC\ D_0$ and $b = \frac{8}{\pi \rho_i D_0^2}$

Integrating over mass and time and differentiating to isolate the time rate of change of mass gives,

$$\frac{dM_T}{dt} = aE_T + \frac{a^2 b E_T^2}{2} t$$

Taking the value of the variables to be represented by those used in the model as follows, in SI units

The diameter	4.67×10^{-2}
The density of ice	890
LWC	$\sim 10^{-3}$
The maximum airspeed	45
Maximum time	600

give $$\frac{dM_T}{dt} = \sim 10^{-4} + \sim 10^{-5}$$

Therefore the second term can be ignored in this formulation when applied to the experimental data used in this thesis.

Appendix 5

Herein is contained a Fortran listing of the model described in Appendix 3.

```
C  ICING OF A CIRCULAR CYLINDER IN LIQUID WATER CONDITIONS
   ONLY
C  ALLOWING FOR RUNBACK
C
C INTERACTIVE PROMPTS FROM MSOURCE FOR LUDLAM LIMIT AND
  GROWTH OPTION
C
C  DATA INPUT FROM MSOURCE BY PROMPTS
C  ALL OTHER DATA FROM LU 2
C
C  INPUT
C
      DIMENSION A(20),B(20),E(20),TH(20),R5(100),AN1(100),
     1          R(100),X(100),Y(100),RWR(100),RWI(100),
     2          AT(50),AP(50)
      REAL LV,LF
      WRITE(6,10)
   10 FORMAT(1H0,'DAY MONTH YEAR',/,'  DD MM YY',/)
      READ(5,20)IDAY,IMON,IYR
   20 FORMAT(3I3)
      WRITE(6,30)
   30 FORMAT(1H0,'ROUGH OR SMOOTH',/,' 1 OR 0 ',/)
      READ(5,40)IRGH
   40 FORMAT(I1)
      WRITE(6,50)
   50 FORMAT(1H0,'SECTOR SIZE IN DEGREES',/,'X.X',/)
      READ(5,60)SECTOR
   60 FORMAT(F3.1)
      WRITE(6,70)
   70 FORMAT(1H0,'DO YOU WANT THE LUDLAM LIMIT',/,'IF NO
     1 JUST "RETURN"',/,'IF YES HIT "1" THEN "RETURN"')
      READ(5,80)IB1
   80 FORMAT(I1)
      WRITE(6,90)
   90 FORMAT(1H0,'DO YOU WANT TO GROW SOME ICE?',/,'IF NO
     1 JUST "RETURN"',/,'IF YES HIT "1" THEN "RETURN"')
      READ(5,100)IB2
  100 FORMAT(I1)
      DO 610 IR=1,57
        WRITE(6,110)
  110   FORMAT(1H0,'ENTER RUN NUMBER E.G. 11',/,'FORMAT I2',
     1 /,'TO END RETURN',/)
        READ(5,120)IRUN
  120   FORMAT(I2)
```

```
      IF(IRUN.EQ.0)GO TO 620
  130 READ(2,140)IA
  140 FORMAT(I2)
      IF(IA .NE. IRUN)GO TO 130
      BACKSPACE 2
      READ(2,150)IA,TA,AL,DC,VL,VH,DV,(A(J),J=1,20)
  150 FORMAT(I2,F5.1,1E9.3,F6.4,3F5.1,20F5.1)
      DATA PR /0.711/,SC /0.595/,LV /2.5E+06/,
     1     CP /1.005E+03/,EP /0.622/,CW /4.27E+03/,
     2     CI /2.07E+03/,RD /287.04/,RI /890.0/,
     3     RW /1.0E+03/
C
C  DISPLAY OF INPUT VARIABLES
C
      WRITE(7,160)IDAY,IMON,IYR
  160 FORMAT(1H1,I2,'/',I2,'/',I2)
      WRITE(7,170)IA
  170 FORMAT(1H0,'RUN NUMBER',I3,/)
      WRITE(7,180)
  180 FORMAT(1H ,6X,'AIR',25X,'CYL',16X,'AIRSPEED',/,5X,'
     1 TEMP(DEG.C)',3X,'LWC(KG/CU.M)',3X,'DIAM(M)',8X,'
     2 LOW/HIGH/INTERVAL)',/)
      WRITE(7,190)TA,AL,DC,VL,VH,DV
  190 FORMAT(1H ,F10.1,1PE17.2,1PE14.3,5X,0PF5.1,'/',F5.1,
     1       '/',F5.1,///)
      WRITE(7,200)SECTOR
  200 FORMAT(1H ,5X,'SECTOR SIZE=',F4.1,' DEGREES',///)
      IF(IRGH .EQ. 1)GO TO 220
      WRITE(7,210)
  210 FORMAT(1H ,5X,'SMOOTH SURFACE HEAT TRANSFER ASSUMED'
     1       ,////)
      GO TO 240
  220 WRITE(7,230)
  230 FORMAT(1H ,5X,'ROUGH SURFACE HEAT TRANSFER ASSUMED',
     1       ////)
  240 WRITE(7,250)
  250 FORMAT(1H ,'DROPLET SPECTRUM PARAMETERS--PERCENT
     1 VOLUME AT GIVEN DIAMETER',/)
      WRITE(7,260)
  260 FORMAT(1H ,5X,'10MU  20MU  30MU  40MU  50MU  60MU
     1 70MU 80MU 90MU 100MU')
      WRITE(7,270)(A(J),J=1,10)
  270 FORMAT(1H ,3X,10F6.1,//)
      WRITE(7,280)
  280 FORMAT(1H ,4X,'110MU 120MU 130MU 140MU 150MU 160MU
     1 170MU 180MU 190MU 200MU')
      WRITE(7,290)(A(J),J=11,20)
  290 FORMAT(1H ,3X,10F6.1)
C
      ICOUNT=AINT((VH-VL)/DV)+1
      V=VL-DV
C
      DO 590 I=1,ICOUNT
         P0=0.96E+05
```

```
            P=P0
            V=V+DV
            WRITE(7,300)V
  300       FORMAT(1H ,/,5X,'FREE STREAM VELOCITY =',F5.1,
     1           '(M/S)',///)
C
C  CALCULATE FUNCTIONS OF AIR TEMPERATURE
C
            RA=P0/(RD*(TA+273.16))
            AM=1.718E-05+5.1E-08*TA
            AK=2.43E-02+7.3E-05*TA
C
C  CALCULATE FUNCTIONS OF VELOCITY
C
            REC=V*DC*RA/AM
            Z8=V*RA/AM
            Z9=RW*V/(9.0*AM*DC)
C
C   CALCULATE LOCAL COLLECTION EFFICIENCY B,TOTAL COLLECTION
C EFFICIENCY, E,
C  AND MAXIMUM IMPINGEMENT ANGLE TH.
C
            DO 320 J=1,20
               AJ=J
               DD=AJ*10.0E-06
               RED=Z8*DD
               AKJ=Z9*DD*DD
               S1=1.0/(1.0+0.0967*(RED**0.6367))
               AK0=0.125+(AKJ-0.125)*S1
               IF(AK0 .LT. 0.125)GO TO 310
               B(J)=1.4*((AK0-0.125)**0.84)
               B(J)=B(J)/(1.0+B(J))
               E(J)=0.489*((ALOG10(8.0*AK0))**1.978)
               TH(J)=ATAN((1.7*(AK0-0.125))**0.76)
               IF(AK0 .LT. 0.9)GO TO 320
               E(J)=AK0/(AK0+1.5708)
               IF(AK0 .LT. 7.5)GO TO 320
               B(J)=AK0/(1.0+AK0)
               IF(AK0 .LT. 10.0)GO TO 320
               TH(J)=ATAN(AK0)
               GO TO 320
  310          E(J)=0.
               B(J)=0.
               TH(J)=1.0E-10
  320       CONTINUE
C
C  CALCULATE FUNCTIONS OF ANGLE AROUND CYLINDER PHI.
C
            N=AINT(90.0/SECTOR)+1
C
            DO 570 II=1,N
               R5(II)=0.0
               RWI(II)=0.0
               RWR(II)=0.0
```

```
                AN1(II)=0.0
                AII=II
                PHI=(AII-1.0)*1.7453E-02*SECTOR
                IF(IRGH .EQ. 1)GO TO 330
                ANU=SQRT(REC)*(1.0-(2.0*PHI/3.1416)**3.0)
                GO TO 340
  330           ANU=SQRT(REC)*(2.4+1.2*SIN(3.6*(PHI-4.3633E-
     1 01)))
  340           H=ANU*AK/DC
                REC=0.75+0.25*COS(2.0*PHI)
                S3=0.
                S4=0.
C
C  CALCULATE COLLECTION EFFICIENCY IN SECTOR I FOR ALL SIZE
C CATEGORIES
C
                DO 350 J=1,20
                    IF(TH(J).LT. PHI)GO TO 350
              G9=B(J)*COS(3.1416*PHI/(2.0*TH(J)))+(31.0063/(
     1        ((TH(J))**3.0)*5.8696))*(E(J)-2.0*TH(J)*B(J)/
     2        3.1416)*PHI*            PHI*SIN(3.1416*PHI/TH(
     3        J))
                    S3=S3+G9*A(J)/100.
                    S4=S4+E(J)*A(J)/100.
  350           CONTINUE
C
C  CALCULATE LUDLAM LIMIT FOR A ROTATING CYLINDER
C
                IF(PHI .NE. 0.)GO TO 390
                IF(IB1 .NE. 1)GO TO 390
                IF(REC .GT. 2.0E+05)GO TO 360
                H0=(AK/DC)*0.229*(REC**0.6)
                GO TO 370
  360           H0=(AK/DC)*0.067*(REC**0.7)
  370           CALL FNE(ESTA,TA)
                CALL FNE(ES0,0.0)
             W1=(-1.0*3.1416*H0*(TA+(ESTA-ES0)*LV*EP*((PR/SC)
     1       **0.63)/(P*CP)+0.4*V*V/(2.0*CP)))/(0.5*V*V+3.
     2       34E+05+CW*TA)
                W2=W1/(S4*V)
                WRITE(7,380)W2
  380        FORMAT(1H ,5X,'CRITICAL LWC FOR A ROTATING
     1CYLINDER (WATER ONLY)  =',1PE10.3,'(KG/M**3)',///)
C
C  LOCAL COLLECTION EFFICIENCY
C
  390           B1=S3
C
C  IMPINGING WATER FLUXES
C
                FW=B1*AL*V
C
C  LOCAL STATIC PRESSURE FOR EVAPORATIVE COOLING TERM
C
```

```
                P=P0+(1.3*COS(2.0*PHI)-0.3)*RA*V*V/2.0
                IF(PHI .EQ. 0.0)GO TO 400
                IF(II .EQ. 2)GO TO 410
                U1=U3
                T7=T0
                GO TO 420
  400           U1=0.0
                T7=0.0
                GO TO 420
  410           U1=U3/2.0
                T7=T0
C
C  ITERATIVE SOLUTION OF HEAT BALANCE EQUATION
C
  420           TS=0.0
  430           DT=TA-TS
                LF=3.34E+05+(CW-CI)*TS
C
C  CALCULATE HEAT TRANSFER TERMS
C
                Q1=H*DT
                CALL FNE(ESTS,TS)
              CALL FNE(ESTA,TA)
                Q2=(ESTA-ESTS)*H*LV*EP*((PR/SC)**0.63)/(P*
     1        CP)
                Q3=FW*CW*DT
                Q5=H*RFC*V*V/(2.0*CP)
                Q6=FW*V*V/2.0
                Y1=U1*CW*(T7-TS)
C
C  TEST FOR NO SPRAY
C
                IF(FW .EQ. 0.0)GO TO 440
                GO TO 460
  440           IF(U1 .EQ. 0.0)GO TO 450
                GO TO 460
  450           AK2=0.0
                AM1=0.0
                F1=0.0
                GO TO 480
  460           IF(TS .LT. 0.0)GO TO 470
                IF(TS .GT. 0.0)GO TO 490
                AK2=1.0
                AM1=0.0
                F1=-1.0*(Q1+Q2+Q3+Q5+Q6+Y1)/(LF*(FW+U1))
                IF(F1 .GT. 1.0)GO TO 470
                IF(F1 .LT. 0.0)GO TO 490
C
C  THERMODYNAMIC ZONE 3
C
                Q4=F1*FW*LF
                Y3=F1*U1*LF
                GO TO 500
C
```

```
C  THERMODYNAMIC ZONE 1
C
  470           F1=1.0
                AK2=0.0
                AM1=0.0
  480           Q4=F1*FW*LF
                Y3=F1*U1*LF
                P9=Q1+Q2+Q3+Q4+Q5+Q6+Y1+Y3
                CALL FNP(PTS,TS)
               PS=-1.0*H-1.0*H*LV*EP*((PR/SC)**0.63)*(PTS/(P*
     1         CP))-FW*CW+F1*FW*(CW-CI)-U1*CW+F1*U1*(CW-CI)
                T9=-1.0*P9/P8
                IF(ABS(T9).LT. 0.01)GO TO 500
                TS=TS+T9
                GO TO 430
C
C  THERMODYNAMIC ZONE 5
C
  490           F1=0.0
                AK2=1.0
                AM1=1.0
                GO TO 480
  500           U3=(1.0-F1)*(FW+U1)
                T0=TS
                RWI(II)=FW
                RWR(II)=U1
                R5(II)=RWI(II)*F1+RWR(II)*F1
                AN1(II)=F1
              R5(II)=R5(II)/.890
                IF(U3 .LT. 0.0)GO TO 600
C
C CHANGE APPROPRIATE QUANTITIES TO RADIAL GROWTH
C
C
C  OUTPUT
C
  510           PHID=PHI*57.296
                IF(PHI .NE. 0.0)GO TO 530
                WRITE(7,520)
  520          FORMAT(1H ,5X,' PHI    N1    TS       RI        RWI
     1         RWR        BETA     QC        QE        QW        YF
     2         QF        QV ,/)
  530          WRITE(7,540)PHID,AN1(II),TS,R5(II),RWI(II),
     1         RWR(II),B1,Q1,Q2,Q3,Y3,Q4,Q5
  540           FORMAT(1H ,5X,F4.0,F6.2,F5.1,3(1PE10.2),
     1             0PF7.2,6(1PE9.1))
  550           FORMAT(1H ,12F6.2)
                IF(R5(II).EQ. 0.0)GO TO 560
                GO TO 570
  560           IF(U3 .EQ. 0.0)GO TO 580
  570          CONTINUE
C
               IF(IB2 .NE. 1)GO TO 590
  580          CALL GROW(N,AN1,R5,RWI,RWR,SECTOR,IA,DC,VL,VH,
```

```
     1          DV)
  590   CONTINUE
  600   REWIND 2
  610 CONTINUE
C
  620 STOP
      END
C
C  SUBROUTINE TO FIND SAT.VAPOUR PRESSURE
C
      SUBROUTINE FNE(ES,T)
      ES=(((2.59E-04*T+2.7487E-02)*T+1.4472)*T+4.426E+01)*T+
     1609.92
      RETURN
      END
C
C  FUNCTION OF P
C
      SUBROUTINE FNP(PS,T)
      PS=((1.036E-03*T+8.2461E-02)*T+2.8944)*T+44.26
      RETURN
      END
```

Appendix 6

The subroutine here listed is called from the main program to calculate ice growth by the directional method.

```
C  THIS SUBROUTINE IS CALLED FROM ICE8.
C
C  PROMPTS MSOURCE FOR TIME OF GROWTH.
C
C
C  GROWTH OCCURS DIRECTIONALLY
C
C
      SUBROUTINE GR(N,SECTOR,IA,R5,DC)
      DIMENSION AN1(100),R5(100),RWI(100),RWR(100),PHD(100),
     1          PHID(100)   ,PHI(100),R(100),TH(100),F(50),
     2          RR(50),PH1(100),G(100),PH1D(100)   ,R1(100),
     3          WO(100),ALPH(100),R2(100),RAX(100),RPX(100)
     4          ,RAY(100),RPY(100)
      WRITE(6,10)
   10 FORMAT(1H ,'ENTER GROWTH TIME(MIN)-TIME STEP(SEC)',/,
     1       'FORMAT 2I2')
      READ(5,20) IT,IDT
   20 FORMAT(2I2)
      AT=IT/2
      AT=AT/10.
      A=IA
      AA=IA+AT
      KK=0
   30 READ(3,40) B
      KK=KK+1
      IF(KK.GT.60)GO TO 250
   40 FORMAT(F4.1)
      IF(B.EQ.AA)GO TO 50
      IF(AA.LT.B.AND.(AA.GT.(B-.05)))GO TO 50
      GO TO 30
   50 BACKSPACE 3
      READ(3,60) B,NN,(RR(I),I=1,NN)
   60 FORMAT(F4.1,I3,50F6.2)
      KF=IT*60/IDT
      ADT=IDT
      DO 70 I=1,N
        G(I)=R5(I)
        RR(I)=RR(I)*10.
        PHID(I)=(I-1)*SECTOR
        PHI(I)=PHID(I)*1.7453E-02
        PH1(I)=PHID(I)*1.7453E-02
        R(I)=DC/.002
        WO(I)=(DC/.002)*SECTOR*1.7453E-02
```

```
   70 CONTINUE
      WO(1)=WO(1)/2.
C
C  TIME-STEPPING
C
      DO 180 K=1,KF
        DT=K*IDT
        T=DT/60.
C
C FIND GROWTH ALONG SECTOR LINE FOR EACH SECTOR
C
        DO 80 I=1,N
          TI=DT/60.
          PH0=37.-TI/2.
          DPHI=PHID(I)-PH0
          SLP=1.8E-04*(TI**4.)-4.64E-03*(TI**3.)+4.77E-02*
     1    TI*TI-.238*TI+1.16
          TH(I)=(DPHI/SLP)*1.7453E-02
   80   CONTINUE
        NM1=N-1
        DO 110 I=1,NM1
          IF(I.NE.1)GO TO 90
          ALPH(1)=0.
          GO TO 100
   90     ALPH(I)=(TH(I)-TH(I-1))/2.
  100     ALPH(I+1)=(TH(I+1)-TH(I))/2.
          TALP=TAN(ALPH(I))+TAN(ALPH(I+1))
          R2(I)=(SQRT(4.*WO(I)*WO(I)+4.*WO(I)*R5(I)*ADT*
     1    TALP)-2.*WO(I))/    (2.*TALP)
          X=R(I)*SIN(PHI(I))+R2(I)*SIN(TH(I))
          Y=R(I)*COS(PHI(I))+R2(I)*COS(TH(I))
          PH1(I)=ATAN2(X,Y)
          R(I)=X/(SIN(PH1(I)))
  110   CONTINUE
        R(N)=R(N-1)
        DO 140 I=1,N
          DO 130 II=1,NN
            IF(PH1(II).LE.PHI(I))GO TO 120
            DRP=(R(II)-R(II-1))/(PH1(II)-PH1(II-1))
            DPH=PH1(II)-PHI(I)
            R1(I)=R(II-1)+DRP*DPH
            GO TO 140
  120       IF(II.NE.NN)GO TO 130
            R1(I)=R(II)
            GO TO 140
  130     CONTINUE
  140   CONTINUE
        DO 170 I=1,NM1
          IF(I.EQ.1)GO TO 150
          B=R1(I)*SECTOR/2.*1.7453E-02
          C=R1(I-1)*SECTOR*1.7453E-02
          WO(I)=SQRT(B*B+(ABS(R1(I+1)-R1(I)))**2.)
     1    +SQRT(C*C+(ABS(R1(I)-R1(I-1)))**2.)
          GO TO 160
```

```
  150       D=R1(1)*SECTOR/2.*1.7453E-02
            WO(1)=SQRT(D*D+(ABS(R1(2)-R1(1)))**2.)
  160       R(I)=R1(I)
  170     CONTINUE
          R(N)=R1(N)
  180 CONTINUE
C
C  DO COMPARISON OF MODEL TO ACTUAL
C
      DO 190 I=1,NN
        F(I)=(R(I)-DC/.002)/(RR(I)-DC/.002)
        RPX(I)=(R(I)/10.)*COS(PHI(I))
        RPY(I)=(R(I)/10.)*SIN(PHI(I))
        RAX(I)=(RR(I)/10.)*COS(PHI(I))
        RAY(I)=(RR(I)/10.)*SIN(PHI(I))
  190 CONTINUE
      WRITE(8,200) IA,T
  200 FORMAT(1H0,'RUN ',I2,' AFTER ',F4.1,' MINUTES',//)
      WRITE(8,210) (PHID(I),I=1,N)
  210 FORMAT(1H ,50F5.1)
      WRITE(8,210) (R(I),I=1,N)
      WRITE(8,210) (RR(I),I=1,NN)
      WRITE(8,220) (F(I),I=1,NN)
  220 FORMAT(1H ,50F5.2)
      WRITE(9,240) IA,NN,(RAX(I),I=1,NN)
      WRITE(9,230) (RAY(I),I=1,NN)
  230 FORMAT(1H ,4X,50F6.3)
      WRITE(9,240) IA,NN,(RPX(I),I=1,NN)
      WRITE(9,230) (RPY(I),I=1,NN)
  240 FORMAT(1H ,2I2,50F6.3)
  250 REWIND 3
      RETURN
      END
```